26 February 2022

Multitask deep active contour-based iris segmentation for off-angle iris images

Tianhao Lu, *Caiyong Wang*, *Yunlong Wang*, *Zhenan Sun (/profile/Zhenan.Sun-51811)*

Author Affiliations + ()

J. of Electronic Imaging, 31(4) (/journals/journal-of-electronic-imaging/volume-31/issue-4), 041211 (2022). https://doi.org/10.1117/1.JEI.31.4.041211 (https://doi.org/10.1117/1.JEI.31.4.041211)

Abstract

Iris recognition has been considered as a secure and reliable biometric technology. However, iris images are prone to off-angle or are partially occluded when captured with fewer user cooperations. As a consequence, iris recognition especially iris segmentation suffers a serious performance drop. To solve this problem, we propose a multitask deep active contour model for off-angle iris image segmentation. Specifically, the proposed approach combines the coarse and fine localization results. The coarse localization detects the approximate position of the iris area and further initializes the iris contours through a series of robust preprocessing operations. Then, iris contours are represented by 40 ordered isometric sampling polar points and thus their corresponding offset vectors are regressed via a convolutional neural network for multiple times to obtain the precise inner and outer boundaries of the iris. Next, the predicted iris boundary results are regarded as a constraint to limit the segmentation range of noise-free iris mask. Besides, an efficient channel attention module is introduced in the mask prediction to make the network focus on the valid iris region. A differentiable, fast, and efficient SoftPool operation is also used in place of traditional pooling to keep more details for more accurate pixel classification. Finally, the proposed iris segmentation approach is combined with off-the-shelf iris feature extraction models including traditional OM and deep learning-based FeatNet for iris recognition. The experimental results on two NIR datasets CASIA-Iris-off-angle, CASIA-Iris-Africa, and a VIS dataset SBVPI show that the proposed approach achieves a significant performance improvement in the segmentation and recognition for both regular and off-angle iris images.

KEYWORDS

Iris recognition

Image segmentation

Eye models

Iris

Feature extraction

Data modeling

Performance modeling

Show All Keywords

1. Introduction

In today's society, biometric identification has become an indispensable part of daily life. As one of the most secure identification modalities, the iris presents unique, stable, and noncontact characteristics. Different individuals and even twins are also completely different. However, traditional iris recognition technology requires high quality of iris images, hence it is difficult to adapt to complex nonconstrained application scenarios. During the process of iris image capture, it is almost impossible to always require the subject to look straight into the camera lens. As a consequence, iris images often suffer from several adverse noise interferences, such as off angle, closed eye, occlusions due to eyelids/glasses, and specular reflections [illegible] is segmentation as well as the subsequent iris recognition. In particular, off-angle iris images are frequently captured, an[illegible]f valid iris pixels, which can be used for identification, as shown in Fig. 1 (/journals/journal-of-electronic-imaging/volume-31/issue[illegible]ctive-contour-based-iris-segmentation-for-off-angle/10.1117/1.JEI.31.4.041211.full#f1). However, there has been currently still a lack of effective iris segmentation models to handle such iris images, hence further improvements are required to increase the utilization rate of iris images.

Fig. 1 Download (/proceedings/DownloadFigures?url=/ContentImages/Journals/JEIME5/31/4/041211/FigureImages/JEI_31_4_041211_f001.png)
Nonconstrained application scenarios and off-angle iris images in near-infrared and visible light illuminations.

Since Daugman[1] (/journals/journal-of-electronic-imaging/volume-31/issue-04/041211/Multitask-deep-active-contour-based-iris-segmentation-for-off-angle/10.1117/1.JEI.31.4.041211.full#r1) proposed the integro-differential operator and Wides[2] (/journals/journal-of-electronic-imaging/volume-31/issue-04/041211/Multitask-deep-active-contour-based-iris-segmentation-for-off-angle/10.1117/1.JEI.31.4.041211.full#r2) proposed the circular Hough transforms, many works[3] (/journals/journal-of-electronic-imaging/volume-31/issue-04/041211/Multitask-deep-active-contour-based-iris-segmentation-for-off-angle/10.1117/1.JEI.31.4.041211.full#r3)–[6] (/journals/journal-of-electronic-imaging/volume-31/issue-04/041211/Multitask-deep-active-contour-based-iris-segmentation-for-off-angle/10.1117/1.JEI.31.4.041211.full#r6) have made improvements and innovations based on them. These methods generally first locate the inner and outer boundaries of the iris, then detect the upper and lower eyelids, and finally eliminate the noise interference of eyelashes, light spots, etc. They have achieved good segmentation performance on some noisy iris images, but they perform poorly in segmenting those seriously off-angle iris images. These methods always assume that inner and outer boundaries of the iris are circular, which is often inconsistent with the actual shape of off-angle iris region. In fact, the boundaries of the off-angle iris images present the more flexible free-form and closed curve. For this reason, some methods also propose elliptic contours,[7] (/journals/journal-of-electronic-imaging/volume-31/issue-04/041211/Multitask-deep-active-contour-based-iris-segmentation-for-off-angle/10.1117/1.JEI.31.4.041211.full#r7) spline,[8] (/journals/journal-of-electronic-imaging/volume-31/issue-04/041211/Multitask-deep-active-contour-based-iris-segmentation-for-off-angle/10.1117/1.JEI.31.4.041211.full#r8) and geodesic active contours[9] (/journals/journal-of-electronic-imaging/volume-31/issue-04/041211/Multitask-deep-active-contour-based-iris-segmentation-for-off-angle/10.1117/1.JEI.31.4.041211.full#r9) to approximate the actual iris boundaries. Despite their flexibility, they are still less robust and adaptable to complex and nonconstrained iris images due to a good initial boundary to be required by them.

In addition to the boundary-based iris segmentation, some methods consider directly predicting the valid iris texture pixels. Tan and Kumar[10] (/journals/journal-of-electronic-imaging/volume-31/issue-04/041211/Multitask-deep-active-contour-based-iris-segmentation-for-off-angle/10.1117/1.JEI.31.4.041211.full#r10) extracted the Zernike moments around pixels as features and then performed classification by SVM to distinguish whether pixels belong to the iris. Radman et al.[11] (/journals/journal-of-electronic-imaging/volume-31/issue-04/041211/Multitask-deep-active-contour-based-iris-segmentation-for-off-angle/10.1117/1.JEI.31.4.041211.full#r11) first localized the iris by the HOG-SVM method and then automatically extracted the iris region by means of a cellular ich evolved under the GrowCut technique. Overall, most of these pixel-based methods isolated[illegible] count the whole structure of the iris region, especially the iris boundary. Besides, they usually ne[illegible] manually, and the training processes of features extraction and classification are separated, thereby it is not ideal to segment nonideal iris images.

With the development of deep learning technologies, many researches have proposed deep learning-based iris segmentation methods. Liu et al.[12] (/journals/journal-of-electronic-imaging/volume-31/issue-04/041211/Multitask-deep-active-contour-based-iris-segmentation-for-off-angle/10.1117/1.JEI.31.4.041211.full#r12) proposed a multiscale hierarchical convolutional neural networks for iris segmentation. Lian et al.[13] (/journals/journal-of-electronic-imaging/volume-31/issue-04/041211/Multitask-deep-active-contour-based-iris-segmentation-for-off-angle/10.1117/1.JEI.31.4.041211.full#r13) introduced an attention mechanism into the U-Net model for iris segmentation. Li et al.[14] (/journals/journal-of-electronic-imaging/volume-31/issue-04/041211/Multitask-deep-active-contour-based-iris-segmentation-for-off-angle/10.1117/1.JEI.31.4.041211.full#r14) proposed an interleaved residual u-net model for iris segmentation. In general, most deep learning-based iris segmentation methods can accurately segment the valid iris region but neglect the localization (or parameterization) of the iris boundaries. Since the latter directly affects the subsequent iris normalization, these methods can not be directly used in typical iris recognition systems. Here, we do not strictly distinguish between iris localization and iris parameterization, because after iris localization detects the complete inner and outer boundaries of the iris, iris parameterization only adds a process of fitting boundaries as circles or ellipses for the subsequent iris normalization. Obviously, iris localization is the most challenging part of iris parameterization, especially for off-angle iris images. Our recent research[15] (/journals/journal-of-electronic-imaging/volume-31/issue-04/041211/Multitask-deep-active-contour-based-iris-segmentation-for-off-angle/10.1117/1.JEI.31.4.041211.full#r15) proposed the IrisParseNet as an effective alternative solution, but it still mainly considered the regular, frontal iris images with circular iris boundaries, and was not specifically designed for off-angle iris images. A similar problem also appeared in the recently published Iris R-CNN,[16] (/journals/journal-of-electronic-imaging/volume-31/issue-04/041211/Multitask-deep-active-contour-based-iris-segmentation-for-off-angle/10.1117/1.JEI.31.4.041211.full#r16) which is a deeply customized Mask R-CNN[17] (/journals/journal-of-electronic-imaging/volume-31/issue-04/041211/Multitask-deep-active-contour-based-iris-segmentation-for-off-angle/10.1117/1.JEI.31.4.041211.full#r17) model specifically for iris segmentation and localization.

To solve the iris segmentation problem for off-angle iris images, we specially improve the traditional active contour methods with deep learning and design a multitask modeling manner to simultaneously achieve the valid iris mask and parameterized inner and outer boundaries of the iris. The proposed method is named *IrisGazeSeg*, which can combine with off-the-shelf iris feature extraction models to form a complete iris recognition pipeline.

In summary, our main contributions can be summarized as follows:

- A multitask deep active contour model IrisGazeSeg is specially designed for the segmentation of off-angle iris images, which combines the traditional active contour models and data-driven deep learning methods. It finally not only segments the valid iris pixels but also achieves the key iris boundary parameterization information for the subsequent iris normalization.

- Compared with the traditional energy optimization-based active contour model, the proposed iris localization branch innovatively adopts the CNN-based regression model to evolve the initial iris contours to the final inner and outer boundaries of the iris. The initial iris contours are obtained through a series of robust preprocessing operations, which reduce the sensitivity of initialization for the regression model.

- A dual-constraint system based on coarse and fine localization results is proposed to refine the iris mask. Besides, efficient channel attention (ECA) and SoftPool are incorporated into the proposed iris segmentation branch to further improve the prediction accuracy of iris mask.

- The experimental results on both near-infrared (NIR) and visible (VIS) datasets show the proposed model is superior to several baseline models in the iris segmentation and localization performance. Besides, it can also be combined with off-the-shelf iris feature extraction models to construct an accurate iris recognition pipeline for processing off-angle iris images. The codes are publicly available at a Github repository: https://github.com/lutianhao/IrisGazeSeg (https://github.com/lutianhao/IrisGazeSeg).

2. Related Work

In this section, we briefly review some important iris segmentation methods, including traditional methods and deep learning-based methods.

2.1. Traditional Methods

Traditional iris segmentation methods mainly utilize classical image processing and pattern recognition models to segment the valid iris region. Pundlik et al.[18] (/journals/journal-of-electronic-imaging/volume-31/issue-04/041211/Multitask-deep-active-contour-based-iris-segmentation-for-off-angle/10.1117/1.JEI.31.4.041211.full#r18) proposed the graph cut method to segment the iris, which was implemented by minimizing an energy function and incorporating the geometry of the eye. Sutra et al.[6] (/journals/journal-of-electronic-imaging/volume-31/issue-04/041211/Multitask-deep-active-contour-based-iris-segmentation-for-off-angle/10.1117/1.JEI.31.4.041211.full#r6) applied the Viterbi algorithm into iris segmentation, where low-resolution images were used to locate rough iris boundaries, and high-resolution images were used to locate fine iris masks. IrisSeg[19] (/journals/journal-of-electronic-imaging/volume-31/issue-04/041211/Multitask-deep-active-contour-based-iris-segmentation-for-off-angle/10.1117/1.JEI.31.4.041211.full#r19) adopted a coarse-to-fine strategy to localize inner and outer iris boundaries. The inner boundary was coarsely detected using an iterative search method to exploit dynamic thresholding and multiple local cues. The outer boundary was first approximated in polar space using adaptive filters and then refined in Cartesian space.

Off-angle iris images are often captured in less-constrained environments, resulting in noncircular and occluded iris boundaries. Such deviation causes many iris segmentation methods that assume a circular shape of an iris boundary fail. To solve this problem, some methods considered the active contours models, which enable the adaptive search for the best edges of a noncircular shape. Shah and Ross.[9] (/journals/journal-of-electronic-imaging/volume-31/issue-04/041211/Multitask-deep-active-contour-based-iris-segmentation-for-off-angle/10.1117/1.JEI.31.4.041211.full#r9) proposed a iris segmentation method based on geodesic active contours. The method can accurately localize the inner and outer iris boundaries in an iterative fashion under the guide of both local and global properties of the image. Banerjee and Mery[7] (/journals/journal-of-electronic-imaging/volume-31/issue-04/041211/Multitask-deep-active-contour-based-iris-segmentation-for-off-angle/10.1117/1.JEI.31.4.041211.full#r7) proposed geodesic active contours and grabcut for iris segmentation and applied ellipse fitting to refine the predicted iris boundaries. Abdullah et al.[20] (/journals/journal-of-electronic-imaging/volume-31/issue-04/041211/Multitask-deep-active-contour-based-iris-segmentation-for-off-angle/10.1117/1.JEI.31.4.041211.full#r20) developed a fusion of an expanding and a shrinking active contour for accurately localize the inner and outer iris boundaries under a new pressure force. Besides the active contours, PS-RANSAC[8] (/journals/journal-of-electronic-imaging/volume-31/issue-04/041211/Multitask-deep-active-contour-based-iris-segmentation-for-off-angle/10.1117/1.JEI.31.4.041211.full#r8) proposed a polar spline RANSAC-based method to locate the inner and outer boundaries of the iris in nonideal iris images, where the Spline curve is used to approximate the iris shape as a closed curve with arbitrary degrees of freedom.

Overall, traditional methods require a large amount of prior experience and manual feature design methods. For the off-angle iris images, the active contours models present promising results, but they are sensitive to initial states and highly depend on the selected convergence policy.[21] (/journals/journal-of-electronic-imaging/volume-31/issue-04/041211/Multitask-deep-active-contour-based-iris-segmentation-for-off-angle/10.1117/1.JEI.31.4.041211.full#r21) Therefore, this paper tries to propose the deep learning-based improved active contour model for better segmenting off-angle iris images.

2.2. Deep Learning-Based Methods

With the development of deep learning, many CNN-based iris segmentation methods, e.g., MFCNs,[12] (/journals/journal-of-electronic-imaging/volume-31/issue-04/041211/Multitask-deep-active-contour-based-iris-segmentation-for-off-angle/10.1117/1.JEI.31.4.041211.full#r12) ATT-UNet,[13] (/journals/journal-of-electronic-imaging/volume-31/issue-04/041211/Multitask-deep-active-contour-based-iris-segmentation-for-off-angle/10.1117/1.JEI.31.4.041211.full#r13) FRED-Net,[22] (/journals/journal-of-electronic-imaging/volume-31/issue-04/041211/Multitask-deep-active-contour-based-iris-segmentation-for-off-angle/10.1117/1.JEI.31.4.041211.full#r22) and PixISegNet,[23] (/journals/journal-of-electronic-imaging/volume-31/issue-04/041211/Multitask-deep-active-contour-based-iris-segmentation-for-off-angle/10.1117/1.JEI.31.4.041211.full#r23) have been proposed and achieved significant improvement over traditional methods in the segmentation accuracy. Specially, considering limited off-angle iris datasets with ground truths, Varkarakis et al.[24] (/journals/journal-of-electronic-imaging/volume-31/issue-04/041211/Multitask-deep-active-contour-based-iris-segmentation-for-off-angle/10.1117/1.JEI.31.4.041211.full#r24) designed a data augmentation methodology to generate a large off-angle iris dataset from a high-quality iris dataset. It further helped develop a low-complexity deep neural network for the off-angle iris segmentation task.

Although CNN-based iris segmentation methods have achieved great success in segmenting the valid iris pixels, they often ignore the parameterization of iris boundaries, which is essential for the subsequent iris normalization typically used for feature extraction. To alleviate this problem, some methods considered circular Hough transform-based iris parameterization[25] (/journals/journal-of-electronic-imaging/volume-31/issue-04/041211/Multitask-deep-active-contour-based-iris-segmentation-for-off-angle/10.1117/1.JEI.31.4.041211.full#r25) or curve fitting-based iris parameterization[26] (/journals/journal-of-electronic-imaging/volume-31/issue-04/041211/Multitask-deep-active-contour-based-iris-segmentation-for-off-angle/10.1117/1.JEI.31.4.041211.full#r26),[27] (/journals/journal-of-electronic-imaging/volume-31/issue-04/041211/Multitask-deep-active-contour-based-iris-segmentation-for-off-angle/10.1117/1.JEI.31.4.041211.full#r27) on the basis of the predicted iris mask. In addition to the postprocessing methods, IrisParseNet[15] (/journals/journal-of-electronic-imaging/volume-31/issue-04/041211/Multitask-deep-active-contour-based-iris-segmentation-for-off-angle/10.1117/1.JEI.31.4.041211.full#r15) jointly modeled the segmentation of iris mask and the localization of iris boundaries in a unified multitask CNN framework. It achieved better iris segmentation and localization performance by reducing the dependence on iris mask in localizing the iris boundaries. The predicted iris boundaries are further parametrized as circles via the circle fitting algorithm for iris normalization. Iris R-CNN[16] (/journals/journal-of-electronic-imaging/volume-31/issue-04/041211/Multitask-deep-active-contour-based-iris-segmentation-for-off-angle/10.1117/1.JEI.31.4.041211.full#r16) assumed the iris boundaries to be double-circle and regarded the segmentation of iris mask and the localization of iris boundaries as an instance segmentation problem. A popular instance segmentation model Mask R-CNN[17] (/journals/journal-of-electronic-imaging/volume-31/issue-04/041211/Multitask-deep-active-contour-based-iris-segmentation-for-off-angle/10.1117/1.JEI.31.4.041211.full#r17) was improved and customized, yielding superior iris segmentation performance. However, they mainly considered the regular, frontal iris images with circular iris boundaries, and were not specifically designed for off-angle iris images. Latest progress involves the 2021 NIR-ISL[28] (/journals/journal-of-electronic-imaging/volume-31/issue-04/041211/Multitask-deep-active-contour-based-iris-segmentation-for-off-angle/10.1117/1.JEI.31.4.041211.full#r28) competition held in IJCB 2021, where a number of deep learning-based approaches have been proposed. The first place team in the competition employed two independent U-Net models to segment the iris mask and iris boundary masks. And a transfer learning-based training procedure was proposed to improve the generalization ability of the model. The inner and outer boundaries of the iris are finally extracted from the predicted iris boundary masks by a mathematical morphology-based edge detection method and further refined by ellipse fitting. The second place team in the competition regarded the iris segmentation and localization as a multiclass segmentation task and proposed an encoder–decoder structure to explicitly exploit the “family” relationship of segmentation regions, so as to mutually promote the iris segmentation and the iris localization. The third place team in the competition employed an improved U-Net model to segment the iris mask, the inner boundary mask of the iris, and the outer boundary mask of the iris simultaneously. Besides, the EfficientNet-B5 was used as the encoder to improve the model’s feature extraction capability; meanwhile, a boundary attention module was proposed to improve the ability of the decoder to pay attention to iris boundaries.

Overall, deep learning-based iris segmentation methods can automatically learn optimal iris features through data-driven end-to-end training. Therefore, they obtain better accuracy and robustness than traditional methods. However, most of the deep learning-based iris segmentation methods have been designed for regular iris images. The specific models for off-angle iris images are lacking. In this paper, we try to solve this problem by combining traditional active contour models and deep learning-based methods.

3. Approach

In this section, we first briefly introduce the whole iris recognition system. Then, we elaborate on the proposed IrisGazeSeg model for off-angle iris image segmentation. The IrisGazeSeg employes a multitask deep active contour model to jointly predict accurate iris segmentation mask, and inner and outer boundaries of the iris. Finally, we present the details of training.

3.1. Pipeline

The pipeline of the whole iris recognition system is shown in Fig. 2 (/journals/journal-of-electronic-imaging/volume-31/issue-04/041211/Multitask-deep-active-contour-based-iris-segmentation-for-off-angle/10.1117/1.JEI.31.4.041211.full#f2), including iris segmentation and localization, normalization, feature extraction, and matching. The specific model structure of IrisGazeSeg is shown in Fig. 3 (/journals/journal-of-electronic-imaging/volume-31/issue-04/041211/Multitask-deep-active-contour-based-iris-segmentation-for-off-angle/10.1117/1.JEI.31.4.041211.full#f3). Specifically, IrisGazeSeg takes the original iris image as the input and simultaneously learns two parallel branches for the segmentation of iris mask and localization of iris boundaries. It may be noted that our IrisGazeSeg is

different from previous methods, e.g., IrisParseNet,[15] (/journals/journal-of-electronic-imaging/volume-31/issue-04/041211/Multitask-deep-active-contour-based-iris-segmentation-for-off-angle/10.1117/1.JEI.31.4.041211.full#r15) the second and third places in 2021 NIR-ISL,[28] (/journals/journal-of-electronic-imaging/volume-31/issue-04/041211/Multitask-deep-active-contour-based-iris-segmentation-for-off-angle/10.1117/1.JEI.31.4.041211.full#r28) which adopted a single fully convolutional network with multiple prediction heads for iris segmentation and localization. We adopt the two main branches equipped with a shared bottom network for multitask learning and pay more attention to accurately locating the inner and outer iris boundaries in addition to the regular pixelwise iris segmentation mask classification.

Fig. 2 Download (/proceedings/DownloadFigures?url=/ContentImages/Journals/JEIME5/31/4/041211/FigureImages/JEI_31_4_041211_f002.png)

Pipeline of an iris recognition system for off-angle iris images, where the proposed IrisGazeSeg is used for iris segmentation, followed by the rubber-sheet-based iris normalization, and finally a feature extraction model is used to extract the iris feature and perform the feature matching.

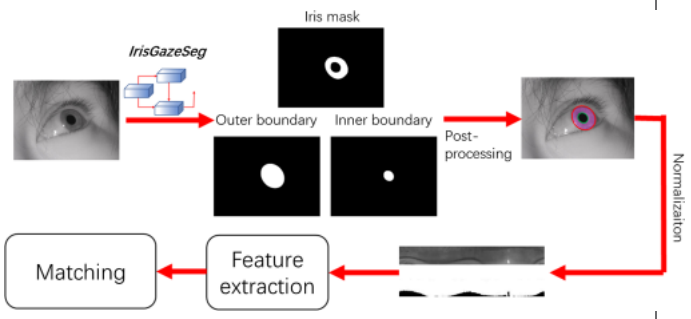

Fig. 3 Download (/proceedings/DownloadFigures?url=/ContentImages/Journals/JEIME5/31/4/041211/FigureImages/JEI_31_4_041211_f003.png)

The architecture of IrisGazeSeg. The upper part shows the localization branch meanwhile the lower part shows the segmentation branch. DACB is introduced in the localization branch to regress the boundary offsets. The postprocessing takes the localization and segmentation predictions to refine the iris mask.

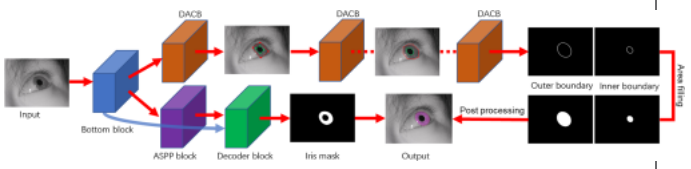

Here, we argue why a single deep learning model may be unsuitable for iris segmentation and localization for off-angle iris images. For the previous single models, each head was required to predict a pixelwise classification map equal to the original image, and it was expected to promote their respective prediction accuracy by mining the proximity relation between the iris mask and iris boundaries. However, when dealing with off-angle iris images, noncircular and occluded iris boundaries would cause a performance drop of the single model. In detail, for unoccluded iris boundary pixels, their segmentation semantics are clear and they are close to the iris segmentation mask. But for occluded iris boundary pixels, their segmentation semantics are fuzzy and they are far from the iris segmentation mask. As a result, the single-model multi-head setting may lead to ambiguity in the semantics for the occluded iris boundary pixels. On the one hand, the iris segmentation head regards them as noniris background pixels due to their deviation from the iris mask, which leads to their nonboundary predictions. On the other hand, the iris localization head still requires predicting them as iris boundary pixels. Therefore, it is often confusing for deep learning models so the occluded iris boundary position needs to be deduced by relying on strong iris structure contextual modeling. However, the noncircular shape of off-angle iris images further makes such deductions harder.

In view of the above considerations, our proposed model not only tends to separate the two predictions earlier but also shares a shallow bottom network in the early stage to reduce the size of the model and obtain some useful common initial features. We also abandon the idea of regarding iris localization as a pixelwise segmentation problem, but holistically consider the iris localization as the regression problem of discrete iris boundary pixels by relying on the prior shape constraint. Specially, we design several deep active contour blocks (DACB) to iteratively regress the offsets of actual iris boundary positions from initial boundary estimations. This manner enables the free-form iris boundary shape modeling and would not be constrained by the regular circular boundaries. The segmentation branch employs Deeplab-like modules to predict the iris mask. The results of localization and segmentation are utilized for refining the iris mask in the postprocessing. To reduce the impact of image resolution and pupil dilation on the iris recognition ability, the iris image and iris mask are then normalized to 512×64 pixels based on the predicted iris boundary parameters. Next, the iris feature is extracted from the normalized iris image. Since iris feature extraction is not the main focus of this paper, we adopt the off-the-shelf iris feature extraction models, including the traditional OM[29] (/journals/journal-of-electronic-imaging/volume-31/issue-04/041211/Multitask-deep-active-contour-based-iris-segmentation-for-off-angle/10.1117/1.JEI.31.4.041211.full#r29) and

deep learning-based FeatNet.[30] (/journals/journal-of-electronic-imaging/volume-31/issue-04/041211/Multitask-deep-active-contour-based-iris-segmentation-for-off-angle/10.1117/1.JEI.31.4.041211.full#r30) Finally, the extracted iris feature is matched with the storied feature templates in the database, where the normalized iris mask is used to ignore the invalid iris pixels during the matching.

3.2. Multitask Deep Active Contour Model

3.2.1. Shared bottom network

The proposed IrisGazeSeg model employes a shared bottom network to extract initial feature representations for both localization and segmentation branch. Specifically, the network is taken from the Mobilenetv2[31] (/journals/journal-of-electronic-imaging/volume-31/issue-04/041211/Multitask-deep-active-contour-based-iris-segmentation-for-off-angle/10.1117/1.JEI.31.4.041211.full#r31) and fine-tuned for different tasks. Besides, considering the low-level features with more details are also beneficial to pixelwise classification, the segmentation branch not only connects the deep features from the final convolutional block but also combines the shallow features from the first convolutional block.

3.2.2. Deep active contour based localization branch

Since the active contour model is ideally suitable to describe the target whose boundary is a free-form closed curve, here we apply it to model the inner and outer boundaries of the iris for off-angle iris images. Given an initial contour, traditional active contour model usually optimizes an energy function with respect to the coordinates of contour points. Then, it drives the coordinates of initial contour vertices toward the actual object boundary by designing proper image forces at the contour coordinates. However, since the energy function is typically nonconvex and depends on handcrafted low-level image features, the deformation process tends to find local optimal solutions. Inspired by the recent Deep Snake,[32] (/journals/journal-of-electronic-imaging/volume-31/issue-04/041211/Multitask-deep-active-contour-based-iris-segmentation-for-off-angle/10.1117/1.JEI.31.4.041211.full#r32) we propose a deep active contour model for the boundary localization of off-angle iris images, which greatly alleviates the problem of traditional active contour models.

In the deep active contour model, we abandon the idea of optimizing the energy function rather than directly learn to evolve the contour from data in an end-to-end manner. Given an initial contour with N vertices $\{x_i|i=1,2,\cdots,N\}$, we first take the concatenation of initially learned features from the share bottom network and the vertex coordinate $[F(x_i);x_i]$ as the feature vector f_i for each vertex x_i. Then from the beginning of this point, we seek to regress a pixelwise vector field from the input image to guide the evolution of the initial contour.

In learning the features of contour points for regression, we model the features on the contour as a periodic signal, which is defined as

Eq. (1)

$$(f_N)_i \triangleq \sum_{j=-\infty}^{\infty} f_{i-jN} = f_{i(\mathrm{mod}\ N)},$$

and encode the periodic features by the circular convolution defined as

Eq. (2)

$$(f_N * k)_i = \sum_{j=-r}^{r} (f_N)_{i+j} k_j,$$

where
$k : [-r, r] \to \mathbb{R}^D$ is a learnable kernel function and the operator
$*$ is the standard convolution.

Based on the circular convolution, we construct a DACB for feature extraction. As shown in Fig. 4 (/journals/journal-of-electronic-imaging/volume-31/issue-04/041211/Multitask-deep-active-contour-based-iris-segmentation-for-off-angle/10.1117/1.JEI.31.4.041211.full#f4), the initial contour points are first taken as the input of DACB, then processed by 8 “CirConv-BN-ReLU” blocks with residual skip connections to extract the features, where “CirConv” represents circular convolution. The extracted multiscale information across all contour points are further fused through a 1×1 convolution layer followed by max pooling. Finally, the fused feature is concatenated with the feature of each vertex and sent to three 1×1 convolution layers to predict vertexwise offsets between contour points and the target points, which are used to deform the contour.

Fig. 4 Download (/proceedings/DownloadFigures?url=/ContentImages/Journals/JEIME5/31/4/041211/FigureImages/JEI_31_4_041211_f004.png)

Detail structures of the localization branch. Initially, two coarse BBox around inner and outer boundaries of the iris are detected and converted to initial inner and outer contours of the iris. In the later refinement process, the DACB takes the ordered sequence composed of contour point coordinates as the input and regresses the offset vector of each contour point. After several rounds of iterative regression, the accurate inner and outer boundaries of the iris are obtained by connecting all ordered contour points.

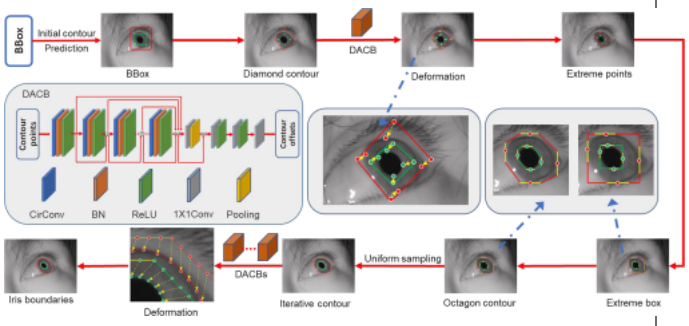

The active contour model is affected by the initial contour of the target, and if the initial contour is closer to the actual position, the prediction would become easier and more accurate. Hence, we design a series of robust preprocessing operations to obtain a good initial iris contour. Specifically, we first employ the CenterNet[33] (/journals/journal-of-electronic-imaging/volume-31/issue-04/041211/Multitask-deep-active-contour-based-iris-segmentation-for-off-angle/10.1117/1.JEI.31.4.041211.full#r33) model to predict the bounding boxes (BBox) around the inner and outer boundaries of the iris. Then, four points centered at the top, left, bottom, and right box borders are extracted and connected to get a diamond contour. To more accurately fit the boundary of the iris, the diamond contour is further deformed by DACB to locate the exposed four extreme points, which are at top, leftmost, bottom, and rightmost in the iris or the pupil boundary, respectively. Next, we construct the octagon contour by generating four lines based on extreme points and connecting their endpoints. To utilize more context information, the octagon contour is uniformly sampled to dense 40 points as the initial iris contour. From the beginning of this, the latter module iteratively regresses 40 offsets by inference multiple times of DACBs, so as to finally obtain the accurate inner and outer boundaries of the iris.

3.2.3. Improved encoder–decoder-based segmentation branch

Inspired by the DeeplabV3+,[34] (/journals/journal-of-electronic-imaging/volume-31/issue-04/041211/Multitask-deep-active-contour-based-iris-segmentation-for-off-angle/10.1117/1.JEI.31.4.041211.full#r34) the segmentation branch adopts an improved encoder–decoder framework by introducing the SoftPool[35] (/journals/journal-of-electronic-imaging/volume-31/issue-04/041211/Multitask-deep-active-contour-based-iris-segmentation-for-off-angle/10.1117/1.JEI.31.4.041211.full#r35) and ECA[36] (/journals/journal-of-electronic-imaging/volume-31/issue-04/041211/Multitask-deep-active-contour-based-iris-segmentation-for-off-angle/10.1117/1.JEI.31.4.041211.full#r36) module. The model architecture of the segmentation branch is shown in Fig. 5 (/journals/journal-of-electronic-imaging/volume-31/issue-04/041211/Multitask-deep-active-contour-based-iris-segmentation-for-off-angle/10.1117/1.JEI.31.4.041211.full#f5). The model consists of the encoder and decoder parts. For the encoder, the deep features from the share bottom network are first sent to the atrous spatial pyramid pooling (ASPP) module to further extract the multiscale semantic features. Then, a 1×1 convolution is operated to fuse these extracted multiscale features. Next, the upsampling operation is performed to expand the feature size. The original ASPP module consists of 3×3 atrous convolutions at rate (1, 6, 12, 18) and a global average pooling followed by the upsampling operation, i.e., P1, P2, P3, P4, and P5 in Fig. 5 (/journals/journal-of-electronic-imaging/volume-31/issue-04/041211/Multitask-deep-active-contour-based-iris-segmentation-for-off-angle/10.1117/1.JEI.31.4.041211.full#f5). Finally, the upsampled deep features from the ASPP and the shallow features from the share bottom network are jointly used in the decoding, which contains four modules, to gradually restore the iris mask. The detailed model parameters of ASPP and four decoding modules (D1, D2, D3, D4) are presented in Table 1 (/journals/journal-of-electronic-imaging/volume-31/issue-04/041211/Multitask-deep-active-contour-based-iris-segmentation-for-off-angle/10.1117/1.JEI.31.4.041211.full#t001).

Fig. 5 Download (/proceedings/DownloadFigures?url=/ContentImages/Journals/JEIME5/31/4/041211/FigureImages/JEI_31_4_041211_f005.png)

Detail structures of the segmentation branch. Input denotes the feature maps from the share bottom network, and Output denotes the predicted segmentation mask. $P_i(i = 1, 2, 3, 4, 5)$ represents different modules in the ASPP, including atrous convolutions with different atrous rates and image pooling. The refined deep features from the ASPP and the shallow features from the share bottom network are jointly used in the decoding to restore the iris mask.

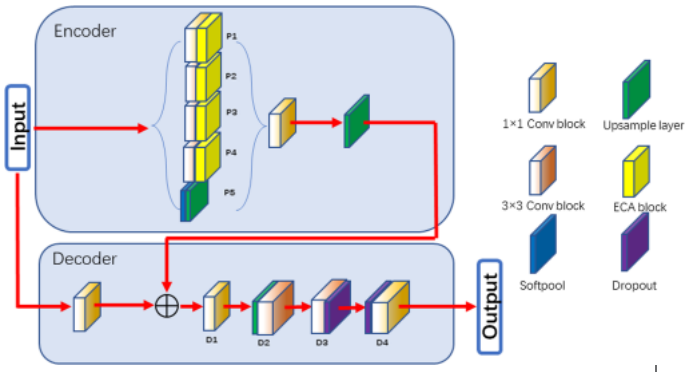

Table 1

Model structure parameters in the segmentation branch.

ASPP	P1	P2	P3	P4	P5
	$\begin{bmatrix}\text{conv 2d}(1\times1,256)\\ \text{BN}\\ \text{ECA}\\ \text{ReLU}\end{bmatrix}$	$\begin{bmatrix}\text{conv 2d}(3\times3,256)\\ \text{BN}\\ \text{ECA}\\ \text{ReLU}\end{bmatrix}$	$\begin{bmatrix}\text{conv 2d}(3\times3,256)\\ \text{BN}\\ \text{ECA}\\ \text{ReLU}\end{bmatrix}$	$\begin{bmatrix}\text{conv 2d}(3\times3,256)\\ \text{BN}\\ \text{ECA}\\ \text{ReLU}\end{bmatrix}$	$\begin{bmatrix}\text{SoftPool}\\ \text{downsample}\end{bmatrix}$
Decoder	D1	D2	D3	D4	—
	$\begin{bmatrix}\text{conv 2d}(1\times1,48)\\ \text{BN}\\ \text{ReLU}\end{bmatrix}$	$\begin{bmatrix}\text{upsample}\times2\\ \text{conv 2d}\ (3\times3,256)\\ \text{BN}\\ \text{ReLU}\end{bmatrix}$	$\begin{bmatrix}\text{dropout}(0.5)\\ \text{conv 2d}(3\times3,256)\\ \text{BN}\\ \text{ReLU}\end{bmatrix}$	$\begin{bmatrix}\text{dropout}(0.1)\\ \text{conv 2d}(1\times1,2)\end{bmatrix}$	

To remain more effective details, we replace the traditional pooling with a recent softpool[35] (/journals/journal-of-electronic-imaging/volume-31/issue-04/041211/Multitask-deep-active-contour-based-iris-segmentation-for-off-angle/10.1117/1.JEI.31.4.041211.full#r35) operation. The SoftPool architecture is shown in Fig. 6 (/journals/journal-of-electronic-imaging/volume-31/issue-04/041211/Multitask-deep-active-contour-based-iris-segmentation-for-off-angle/10.1117/1.JEI.31.4.041211.full#f6). Specifically, each element before pooling contributes to the result of pooling. It retains the basic attributes and amplifies the activation of features with greater intensity. In the backpropagation, a gradient can be provided for each input element. The SoftPool is differentiable when compared with the traditional pooling. Supposed that the pooling size is 2, it is formulated as follows:

Eq. (3)

$$P_{\text{final}} = \sum_{i=1}^{4}\left(P_i \times \frac{e^{P_i}}{\sum_{j=1}^{4} e^{P_j}}\right),$$

where

P denotes the value of the participating pooled pixel points.

Fig. 6 Download (/proceedings/DownloadFigures?url=/ContentImages/Journals/JEIME5/31/4/041211/FigureImages/JEI_31_4_041211_f006.png)

Schematic diagram of SoftPool. P_i represents the pixel value $(i = 1,2,3,4)$; different colors indicate unequal values for different pixels.

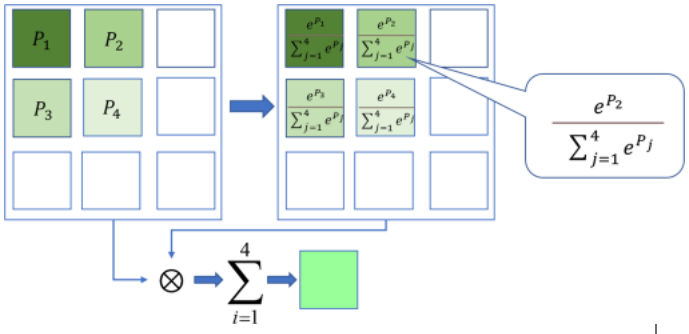

In addition, we introduce the ECA[36] (/journals/journal-of-electronic-imaging/volume-31/issue-04/041211/Multitask-deep-active-contour-based-iris-segmentation-for-off-angle/10.1117/1.JEI.31.4.041211.full#r36) module to focus on the important regions for iris segmentation. The architecture of ECA is shown in Fig. 7 (/journals/journal-of-electronic-imaging/volume-31/issue-04/041211/Multitask-deep-active-contour-based-iris-segmentation-for-off-angle/10.1117/1.JEI.31.4.041211.full#f7). It makes a clear improvement about the Squeeze-and-excitation networks.[37] (/journals/journal-of-electronic-imaging/volume-31/issue-04/041211/Multitask-deep-active-contour-based-iris-segmentation-for-off-angle/10.1117/1.JEI.31.4.041211.full#r37) As a lightweight module, ECA greatly improves the performance of the model while introducing fewer parameters. The mechanism improves the performance and efficiency of the channel attention from the perspective of avoiding dimensional reduction and appropriate cross-channel interaction. In this paper, we append this module to the ASPP and combine with different-scale convolutional layers. The newly added ECA module is expected to focus on the area of greater interest and meanwhile suppress irrelevant noise region. In the ECA module, the choice of the channel number K is determined by an adaptive method, formulated as follows:

Eq. (4)

$$k = \psi(C) = \left| \frac{\log_2(C)}{\gamma} + \frac{b}{\gamma} \right|_{\text{odd}},$$

where
$|t|_{\text{odd}}$ is the nearest odd number,
γ,
b are the hyperparameters, which are set to 2 and 1, respectively.

Fig. 7 Download (/proceedings/DownloadFigures?url=/ContentImages/Journals/JEIME5/31/4/041211/FigureImages/JEI_31_4_041211_f007.png)
The ECA module ($K = 3$).

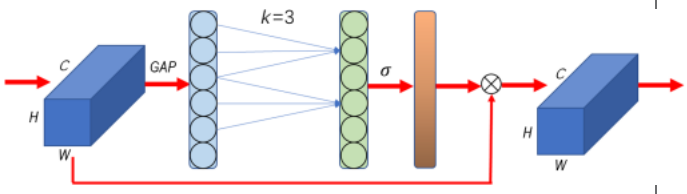

Fig. 8 Download (/proceedings/DownloadFigures?url=/ContentImages/Journals/JEIME5/31/4/041211/FigureImages/JEI_31_4_041211_f008.png)
The postprocessing procedure based on different η. The blue curve represents the ground-truth iris boundary. The rectangular box represents the BBox of iris. The red curve represents the predicted iris boundaries. The yellow region represents the predicted iris mask.

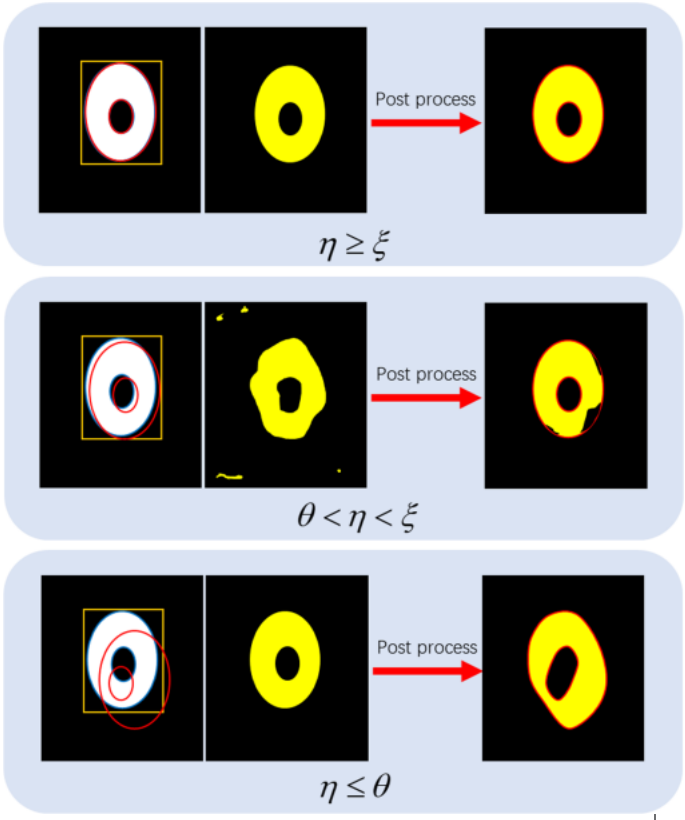

3.2.4. Postprocessing

After obtaining the iris localization and segmentation results, we further refine both predictions through an effective postprocessing procedure, as shown in Fig. 8 (/journals/journal-of-electronic-imaging/volume-31/issue-04/041211/Multitask-deep-active-contour-based-iris-segmentation-for-off-angle/10.1117/1.JEI.31.4.041211.full#f8). For the iris localization branch, we have achieved the coarse-gained BBoxes predicted by CenterNet[33] (/journals/journal-of-electronic-imaging/volume-31/issue-04/041211/Multitask-deep-active-contour-based-iris-segmentation-for-off-angle/10.1117/1.JEI.31.4.041211.full#r33) and fine-gained iris boundaries (contours) predicted by the deep active contour method. For the iris segmentation branch, we have obtained the pixelwise binary iris mask, where the valid iris pixel region is denoted as MI. By comparing the positions of iris boundaries and iris mask, we divide the pixel points in the MI into two categories: inside the boundary and outside the boundary, denoted as MI_{in} and MI_{out}, respectively, i.e., $MI = MI_{\text{in}} + MI_{\text{out}}$. Note that there may be some misclassified pixel points far away from the actual iris region, which are excluded by determining whether being inside the BBox. Hence, we assume that MI, MI_{in}, MI_{out} has ruled out the above types of pixels.

Then we calculate $\eta = MI_{\text{in}}/MI$, which denotes the proportion of iris pixels enclosed by inner and outer boundaries of the iris to total predicted iris pixels. Furthermore, we set two decision thresholds θ and ξ, where $\xi > \theta$. According to the value of η, we adopt different processing strategies as follows: (1) when $\eta \geqslant \xi$, the localization and segmentation results are empirically considered to be accurate, hence no postprocessing is needed; (2) when $\theta < \eta < \xi$, the localization result is considered to be accurate, but the segmentation result may be inaccurate. As a result, we only keep the pixel points enclosed by inner and outer boundaries of the iris as the final segmentation result; (3) when $\eta \leqslant \theta$, there are two possibilities, one of which is that the segmentation result is accurate while the localization result is inaccurate, and the other is that both the segmentation and localization results are inaccurate. Under this circumstance, we take the union of the segmentation result and the loop region of the localized iris boundaries as the final segmentation result. And we extract the boundary of the new segmented region as the final inner and outer boundaries of the iris. Finally, iris boundaries are parameterized via the ellipse fitting algorithm for the subsequent iris normalization.

3.3. Training Details

We simultaneously optimize all the outputs of the network in an end-to-end manner. In particular, we respectively formulate the corresponding loss function for the branch of iris localization and segmentation. Then, the overall loss function is summarized as follows:

Eq. (5)

$$L_{\text{total}} = \beta L_{\text{boundary}} + \gamma L_{\text{mask}}.$$

For the training of the localization branch, we use the smooth l_1 loss[38] (/journals/journal-of-electronic-imaging/volume-31/issue-04/041211/Multitask-deep-active-contour-based-iris-segmentation-for-off-angle/10.1117/1.JEI.31.4.041211.full#r38) to learn the two deformation processes and Bbox, i.e., $L_{\text{boundary}} = L_{\text{ex}} + L_{\text{snake}} + L_{\text{BBox}}$. The loss function for extreme point prediction is defined as

Eq. (6)

$$L_{\text{ex}} = \frac{1}{4}\sum_{i=1}^{4} l_1(\tilde{x}_i^{\text{ex}} - x_i^{\text{ex}}),$$

where
$\tilde{x}_i^{\text{ex}}$ is the predicted extreme point. And the loss function for iterative contour deformation is defined as

Eq. (7)

$$L_{\text{snake}} = \frac{1}{N}\sum_{i=1}^{N} l_1(\tilde{x}_i - x_i^{\text{gt}}),$$

where
$\tilde{x}_i$ is the deformed contour point and
x_i^{gt} is the ground-truth boundary point. Similarly, the loss function of Bbox is defined as

Eq. (8)

$$L_{\text{BBox}} = \frac{1}{4}\sum_{i=1}^{4} l_1(\tilde{x}_i^{\text{Bbox}} - x_i^{\text{Bbox}}),$$

where
$\tilde{x}_i^{\text{Bbox}}$ is the predicted corner points of Bbox. Since CenterNet predictions are represented by Bbox center coordinates, width, and height, we convert it into corner coordinates. The
β is set to 1.

For the training of the segmentation branch, considering that the pixelwise classification categories are unbalanced, where the negative noniris pixels are far more than positive iris pixels, we use the focal loss[39] (/journals/journal-of-electronic-imaging/volume-31/issue-04/041211/Multitask-deep-active-contour-based-iris-segmentation-for-off-angle/10.1117/1.JEI.31.4.041211.full#r39) to learn the segmentation process and alleviate this problem. The loss function is defined as

Eq. (9)

$$L_{\text{mask}}(\mathrm{M}) = -(1-M)^{\varphi}\,\log(M),$$

where
$M(x, y)$ denotes the binary map of the segmentation result, and
φ is a tuned weight parameter, set to 2. Besides, the
γ is set to 1 in the training.

4. Experiment

In this section, we first introduce the dataset and baselines in Sec. 4.1 (/journals/journal-of-electronic-imaging/volume-31/issue-04/041211/Multitask-deep-active-contour-based-iris-segmentation-for-off-angle/10.1117/1.JEI.31.4.041211.full#sec4.1). Second, the implementation details of the model are presented in Sec. 4.2 (/journals/journal-of-electronic-imaging/volume-31/issue-04/041211/Multitask-deep-active-contour-based-iris-segmentation-for-off-angle/10.1117/1.JEI.31.4.041211.full#sec4.2). Third, we describe the evaluation metrics for iris localization, iris segmentation, and iris recognition in Sec. 4.3 (/journals/journal-of-electronic-imaging/volume-31/issue-04/041211/Multitask-deep-active-contour-based-iris-segmentation-for-off-angle/10.1117/1.JEI.31.4.041211.full#sec4.3). Finally, we analyze the experimental results in Sec. 4.4 (/journals/journal-of-electronic-imaging/volume-31/issue-04/041211/Multitask-deep-active-contour-based-iris-segmentation-for-off-angle/10.1117/1.JEI.31.4.041211.full#sec4.4).

4.1. Datasets and Baselines

To evaluate the performance of IrisGazeSeg in different scenarios, we perform the experiments on three diverse off-angle iris image datasets, including SBVPI,[40] (/journals/journal-of-electronic-imaging/volume-31/issue-04/041211/Multitask-deep-active-contour-based-iris-segmentation-for-off-angle/10.1117/1.JEI.31.4.041211.full#r40) CASIA-Iris-Off-angle,[41] (/journals/journal-of-electronic-imaging/volume-31/issue-04/041211/Multitask-deep-active-contour-based-iris-segmentation-for-off-angle/10.1117/1.JEI.31.4.041211.full#r41) and CASIA-Iris-Africa.[28] (/journals/journal-of-electronic-imaging/volume-31/issue-04/041211/Multitask-deep-active-contour-based-iris-segmentation-for-off-angle/10.1117/1.JEI.31.4.041211.full#r28) Besides, we specially select two methods PS-RANSAC[8] (/journals/journal-of-electronic-imaging/volume-31/issue-04/041211/Multitask-deep-active-contour-based-iris-segmentation-for-off-angle/10.1117/1.JEI.31.4.041211.full#r8) and IrisSeg[19] (/journals/journal-of-electronic-imaging/volume-31/issue-04/041211/Multitask-deep-active-contour-based-iris-segmentation-for-off-angle/10.1117/1.JEI.31.4.041211.full#r19) for comparisons. These two methods are better at processing off-angle iris images than other public methods, hence they are suitable as the baselines. Main characteristics of the datasets are summarized in Table 2 (/journals/journal-of-electronic-imaging/volume-31/issue-04/041211/Multitask-deep-active-contour-based-iris-segmentation-for-off-angle/10.1117/1.JEI.31.4.041211.full#t002).

Table 2

Overview of the datasets used in this work. Each of these is a subset of the corresponding original database.

Dataset	No. of iris images	Light source	Environment	Resolution (pixels)
SBVPI	1233	VIS	Indoor	300×170
CASIA-Iris-Off-angle	500	NIR	Indoor	640×480
CASIA-Iris-Africa	740	NIR	Indoor	1088×640

SBVPI consists of 1858 RGB eye images captured in visible light with a resolution of 300×170 from 55 subjects. In this paper, we select the 1233 off-angle iris images as the experimental subset, where 616 iris images are used for training, and the remaining 617 images are used for testing. Some sample images in the SBVPI dataset are shown in Fig. 9(a) (/journals/journal-of-electronic-imaging/volume-31/issue-04/041211/Multitask-deep-active-contour-based-iris-segmentation-for-off-angle/10.1117/1.JEI.31.4.041211.full#f9).

Fig. 9 Download (/proceedings/DownloadFigures?url=/ContentImages/Journals/JEIME5/31/4/041211/FigureImages/JEI_31_4_041211_f009.png)

Examples of the used dataset: (a) SBVPI, (b) CASIA-Iris-Off-angle, and (c) CASIA-Iris-Africa.

CASIA-Iris-Off-angle collects 500 off-angle iris images from Asian subjects. The original iris images contain partial faces, hence the eye region is manually extracted at 640×480 pixels resolution for each selected image. In the experiment, 100 iris images are randomly selected for training, whereas the rest 400 iris images are used for testing. Some sample images in the CASIA-Iris-Off-angle dataset are shown in Fig. 9(b) (/journals/journal-of-electronic-imaging/volume-31/issue-04/041211/Multitask-deep-active-contour-based-iris-segmentation-for-off-angle/10.1117/1.JEI.31.4.041211.full#f9).

CASIA-Iris-Africa contains 740 African iris images collected in NIR illumination with the resolution of 640×480 pixels, which are mostly off-angle. In the experiment, 370 images are randomly selected to form the training set, and the remaining 370 images are used for testing. Some sample images in the CASIA-Iris-Africa dataset are shown in Fig. 9(c) (/journals/journal-of-electronic-imaging/volume-31/issue-04/041211/Multitask-deep-active-contour-based-iris-segmentation-for-off-angle/10.1117/1.JEI.31.4.041211.full#f9).

4.2. Implementation Details

The proposed model is implemented in PyTorch on one Tesla V100 GPU. Due to the limited number of the training samples, heavy data augmentation is performed to expand the training set. In detail, the augmentation operations consist of (1) randomly rotating the image (and ground-truth maps) by a uniform factor between -30 and 30, (2) randomly resizing the image (and ground-truth maps) to three scales (0.5,1,1.5), (3) randomly left or right flipping the image (and ground-truth maps), and (4) adding Gaussian noise to the image. In the training, we use Adam to optimize the network with a minibatch of 4 and L_2 weights regularization coefficient of 1×10^{-8} for 300 epoches. The learning rate is initialized as 1×10^{-4} and drops by half at 80, 120, 200, and 240 epochs. In the postprocessing, the decide threshold θ and ξ are set to 0.3 and 0.9, respectively.

For the PS-RANSAC, we use its public codes (available at a Github repository: https://github.com/DonidaLabati/PS-RANSAC (https://github.com/DonidaLabati/PS-RANSAC)) for experiments, where four points of the inner iris boundary are required to manually labeled in advance so as to assist estimating a circle approximating the inner iris boundary. For the IrisSeg, we use its public codes (available at a Github repository:

https://github.com/Abhishek-MLDL/IrisSeg (https://github.com/Abhishek-MLDL/IrisSeg)) for experiments, where the iris mask, and iris inner, and outer circles are obtained. For top three algorithms in NIR-ISL competition, we use their public codes and trained models (available at a Github repository: https://github.com/xiamenwcy/NIR-ISL-2021 (https://github.com/xiamenwcy/NIR-ISL-2021)) for testing. Specially, the CASIA-Iris-Africa pretrained model is used to test the red-channel iris image in SBVPI datasets.

4.3. Evaluation Metrics

The performance of the proposed model is evaluated from multiple aspects including iris localization, iris segmentation, iris recognition, running time, and model complexity. Specially, the metric values of iris localization and iris segmentation are computed based on the predicted binary iris boundary or iris mask and the manually labeled ground truths.

4.3.1. Iris localization

The Hausdorff distance is used to evaluate the shape similarity of the predicted and ground-truth iris boundary, defined as follows:

Eq. (10)

$$H(GT, P) = \max\{\sup_{x \in GT} \inf_{y \in P} \|x - y\|, \sup_{x \in P} \inf_{y \in GT} \|x - y\|\},$$

where
GT represents the ground-truth iris boundary and
P represents the predicted iris boundary. Furthermore, the Hausdorff distance is normalized by the horizontal eye width to make the boundary results at different image or iris size comparable.

Smaller Hausdorff distances correspond to higher shape similarity between the predicted and ground-truth iris boundary, suggesting higher localization accuracy. We calculate the mean Hausdorff distance (mHdis) for the inner or outer iris boundaries, respectively, and then take their average value as the overall accuracy of iris localization. In addition, the varying iris localization success rates are calculated by setting different thresholds with respect to the Hausdorff distance, and thus a percentage of correct localization (PCL) curve is drawn. On this basis, we further calculate the area-under-the-curve (AUC) corresponding to the maximum threshold (τ), i.e., $\mathrm{AUC}\,@\tau$.

4.3.2. Iris segmentation

Following the NICE.I[42] (/journals/journal-of-electronic-imaging/volume-31/issue-04/041211/Multitask-deep-active-contour-based-iris-segmentation-for-off-angle/10.1117/1.JEI.31.4.041211.full#r42) competition, we adopt the $E1$ and $E2$ as the evaluation metrics for iris segmentation. Specifically, the $E1$ represents the average segmentation error rate, formulated as follows:

Eq. (11)

$$E1 = \frac{1}{n \times c \times r} \sum_{c'} \sum_{r'} G(c', r') \otimes M(c', r'),$$

where
n, r, c denote the number, height (number of rows), and width (number of columns) of the testing image, respectively,
G, M denote the ground-truth and predicted iris mask, respectively,
c', r' denote the column and row coordinates of the pixel points in
G and
M, respectively, and the operator
$\otimes$ denotes the logical XOR operation to evaluate the inconsistent pixels in
G and
M.

$E2$ is proposed to compensate the disproportion between the priori probabilities of iris and noniris pixels in the images. It averages the false-positive rate fp and false-negative rate fn as follows:

Eq. (12)

$$E2 = \frac{1}{2 \times n} \sum_{i} (fp + fn),$$

where
n denotes the number of testing images.

Furthermore, we also report a common semantic segmentation metric $F1$, which is defined as the harmonic mean of precision and recall:

Eq. (13)

$$F1 = \frac{2RP}{R + P},$$

where
R represents the recall rate and
P represents the accuracy rate.

4.3.3. Iris recognition

We also evaluate the performance of iris recognition when the proposed model serves as a drop-in replacement for iris segmentation and localization. The equal error rate (EER) is reported. The DET curve is also drawn according to the FNMR@FMR. Lower EER indicates better recognition performance. When the model has a lower FNMR at a specific FMR (i.e., 10^{-3}), it indicates better model stability.

4.4. Experimental Results and Analysis

4.4.1. Iris localization

First, the visual comparison results are shown in Fig. 10 (/journals/journal-of-electronic-imaging/volume-31/issue-04/041211/Multitask-deep-active-contour-based-iris-segmentation-for-off-angle/10.1117/1.JEI.31.4.041211.full#f10). As can be seen, the proposed IrisGazeSeg can predict the accurate inner and outer boundaries of the iris for regular and off-angle iris images. However, the PS-RANSAC tends to locate the exposed iris boundaries, which ignores the iris part under the occlusion of eyelids. The IrisSeg predicts the circles to describe the iris inner and outer boundaries, which are inconsistent with the actual boundary of off-angle iris images. As for the top-three deep learning-based methods in NIR-ISL, they simply treat the iris localization problem as a segmentation task, but not consider the nature property of iris boundary itself and the challenge of off-angle iris images. Specifically, for the second and third place methods, the single-model multihead setting does not lead to the accurate iris localization results, especially in the occluded iris boundary parts. In contrast, the first place method works better, but it completely uses two independent U-Net models to segment the iris mask and iris boundary masks, which ignores *a priori* positional relationship between them and results in a large computational burden. Interestingly, it also confirms that the single-model multihead setting may be disadvantageous from the reverse side.

Fig. 10 Download (/proceedings/DownloadFigures?url=/ContentImages/Journals/JEIME5/31/4/041211/FigureImages/JEI_31_4_041211_f010.png)
Samples of iris localization results from IrisGazeSeg (ours) and five baselines on different datasets. The ground-truth iris boundaries are also presented for convenient comparison. The inner boundary of the iris is labeled in red while the outer boundary of the iris is labeled in green.

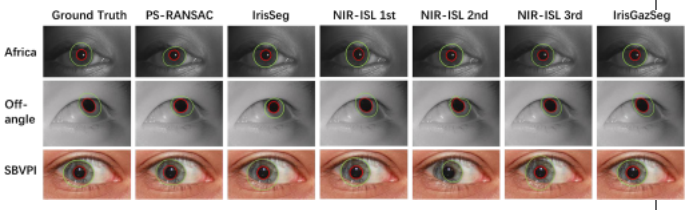

Second, the quantitative comparison results are shown in Table 3 (/journals/journal-of-electronic-imaging/volume-31/issue-04/041211/Multitask-deep-active-contour-based-iris-segmentation-for-off-angle/10.1117/1.JEI.31.4.041211.full#t003). From the results, it can be seen that the proposed IrisGazeSeg clearly outperforms both baselines in term of multiple localization metrics. Furthermore, the PCL curve in Fig. 11 (/journals/journal-of-electronic-imaging/volume-

31/issue-04/041211/Multitask-deep-active-contour-based-iris-segmentation-for-off-angle/10.1117/1.JEI.31.4.041211.full#f11) also indicates that under different thresholds, our proposed IrisGazeSeg has a better detection success rate than the compared five baselines.

Table 3

Comparison of different methods on the iris localization.

Method	Datasets	Inner mHdis (%)	Outer mHdis (%)	Overall mHdis (%)	AUC@0.3
	SBVPI	1.7731	2.4542	2.1137	0.2579
PS-RANSAC	CASIA-Iris-Off-angle	1.6845	3.1468	2.4157	0.2585
	CASIA-Iris-Africa	1.7779	4.7437	3.2608	0.2537
	SBVPI	1.6845	2.7233	2.2039	0.2566
IrisSeg	CASIA-Iris-Off-angle	2.4134	3.4247	2.9191	0.2613
	CASIA-Iris-Africa	1.9549	3.3938	2.6744	0.2684
	SBVPI	1.4716	1.8612	1.6664	0.2832
The first in NIR-ISL	CASIA-Iris-Off-angle	1.2492	1.9647	1.6070	0.2762
	CASIA-Iris-Africa	0.9431	**0.9003**	0.9217	0.2873
	SBVPI	1.8964	2.1360	2.0162	0.2703
The second in NIR-ISL	CASIA-Iris-Off-angle	1.4727	2.2123	1.8425	0.2738
	CASIA-Iris-Africa	0.9412	0.9826	0.9619	0.2824
	SBVPI	1.6168	2.1347	1.8758	0.2864
The third in NIR-ISL	CASIA-Iris-Off-angle	1.7913	2.0248	1.9081	0.2794
	CASIA-Iris-Africa	0.9328	0.9127	0.9228	0.2893
	SBVPI	**0.9453**	**0.9275**	**0.9364**	**0.2971**
Ours	CASIA-Iris-Off-angle	**0.9546**	**0.9237**	**0.9392**	**0.2854**
	CASIA-Iris-Africa	**0.9303**	0.9082	**0.9193**	**0.2901**

Note: Bold font indicates the best performance in a column.

Fig. 11 Download (/proceedings/DownloadFigures?url=/ContentImages/Journals/JEIME5/31/4/041211/FigureImages/JEI_31_4_041211_f011.png)

Performance comparison of iris localization for different methods using the PCL curve. Detection success rate is thresholded on the Hausdorff distance error normalized by horizontal eye width.

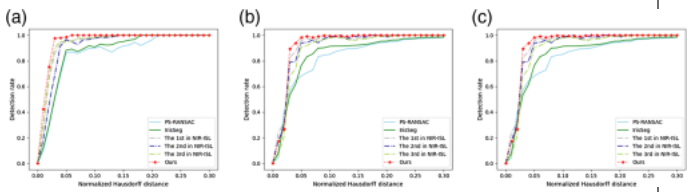

Overall, qualitative and quantitative results prove the superiority of our proposed IrisGazeSeg on the iris localization. More importantly, compared with some recent CNN-based iris segmentation models, our proposed IrisGazeSeg provides critical boundary information for the subsequent iris normalization.

4.4.2. Iris segmentation

Similarly, we first visualize the segmentation results of different iris segmentation methods on several regular and off-angle iris images, as shown in Fig. 12 (/journals/journal-of-electronic-imaging/volume-31/issue-04/041211/Multitask-deep-active-contour-based-iris-segmentation-for-off-angle/10.1117/1.JEI.31.4.041211.full#f12). It can be seen that IrisSeg and PS-RANSAC suffer from poor segmentation results. The deep learning methods in NIR-ISL achieve a relatively good performance on CASIA-Iris-Off-angle and CASIA-Iris-Africa datasets. But only the first place performs well on the SBVPI dataset. A part of the reason is that the first place employes the transfer learning strategy to present better cross-database performance than other two methods. However, our proposed IrisGazeSeg consistently presents the accurate segmentation results on different samples.

Fig. 12 Download (/proceedings/DownloadFigures?url=/ContentImages/Journals/JEIME5/31/4/041211/FigureImages/JEI_31_4_041211_f012.png)

Samples of iris segmentation results from IrisGazeSeg (ours) and five baselines on different datasets. The ground-truth iris mask (the second column) is also presented for convenient comparison.

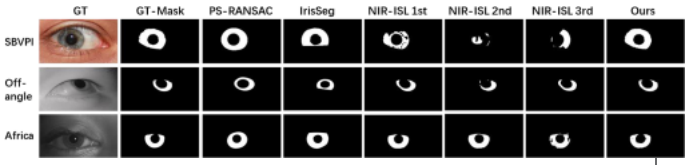

Table 4 (/journals/journal-of-electronic-imaging/volume-31/issue-04/041211/Multitask-deep-active-contour-based-iris-segmentation-for-off-angle/10.1117/1.JEI.31.4.041211.full#t004) quantitatively compares the performance of the proposed IrisGazeSeg with baseline methods on iris segmentation. We can see that IrisGazeSeg has achieved clear performance advantages over baselines on CASIA-Iris-Off-angle and SBVPI datasets and is competitive with the optimal method on the CASIA-Iris-Africa dataset. Therefore, qualitative and quantitative results prove the superiority of our proposed IrisGazeSeg on the iris segmentation.

Table 4

Comparison of different methods on the iris segmentation.

Method	Datasets	E1 (%)	E2 (%)	F1 (%)
	SBVPI	3.51	1.76	87.24
PS-RANSAC	CASIA-Iris-Off-angle	1.92	0.96	89.13
	CASIA-Iris-Africa	2.46	1.23	87.71
	SBVPI	4.72	3.86	86.58
IrisSeg	CASIA-Iris-Off-angle	1.39	0.70	89.64
	CASIA-Iris-Africa	1.80	0.90	89.32
	SBVPI	2.67	1.09	88.17
The first in NIR-ISL	CASIA-Iris-Off-angle	0.69	0.35	93.15
	CASIA-Iris-Africa	**0.61**	**0.31**	**93.87**
	SBVPI	4.21	2.10	86.20
The second in NIR-ISL	CASIA-Iris-Off-angle	0.93	0.53	91.37
	CASIA-Iris-Africa	0.59	0.29	94.37
	SBVPI	3.26	1.13	87.93
The third in NIR-ISL	CASIA-Iris-Off-angle	0.73	0.37	92.76
	CASIA-Iris-Africa	1.17	0.59	91.07
	SBVPI	**0.89**	**0.37**	**91.43**
Ours	CASIA-Iris-Off-angle	**0.67**	**0.35**	**93.37**
	CASIA-Iris-Africa	0.71	0.51	92.36

Note: Bold font indicates the best performance in a column.

4.4.3. Iris recognition

In the iris recognition experiments, we use the full set of CASIA-Iris-Off-angle, which consists of 1446 iris images from 233 subjects. Each subject contains left and right iris images. During the performance evaluation, the left and right eyes are treated as different individuals, hence there are 466 categories to be classified. Furthermore, we use the traditional OM[29] (/journals/journal-of-electronic-imaging/volume-31/issue-04/041211/Multitask-deep-active-contour-based-iris-segmentation-for-off-angle/10.1117/1.JEI.31.4.041211.full#r29) and deep learning-based FeatNet[30] (/journals/journal-of-electronic-imaging/volume-31/issue-04/041211/Multitask-deep-active-contour-based-iris-segmentation-for-off-angle/10.1117/1.JEI.31.4.041211.full#r30) as the iris feature extractor to extract the iris feature and perform the matching. Therefore, the iris segmentation and localization method becomes the unique comparison variable to fairly evaluate their impact on the iris recognition.

The experimental results are shown in Table 5 (/journals/journal-of-electronic-imaging/volume-31/issue-04/041211/Multitask-deep-active-contour-based-iris-segmentation-for-off-angle/10.1117/1.JEI.31.4.041211.full#t005) and Fig. 13 (/journals/journal-of-electronic-imaging/volume-31/issue-04/041211/Multitask-deep-active-contour-based-iris-segmentation-for-off-angle/10.1117/1.JEI.31.4.041211.full#f13). It can be seen that the proposed IrisGazeSeg model is superior to all baseline models on the EER for both iris feature extractors. Besides, the proposed IrisGazeSeg also consistently presents a lower FNMR at different FMR in the DET curve, suggesting a better recognition performance. Moreover, the recognition results also show that the proposed IrisGazeSeg does not depend on a specific iris feature extraction model and is consistently effective when used along with different models.

Table 5

Comparison of different methods on the iris recognition.

Datasets	Method	EER

CASIA-Iris-Off-angle	PS-RANSAC (FeatNet)	0.4342
	IrisSeg (FeatNet)	0.4094
	The third in NIR-ISL (OM)	0.2281
	The third in NIR-ISL (FeatNet)	0.2137
	The second in NIR-ISL (OM)	0.2087
	The second in NIR-ISL (FeatNet)	0.2073
	The first in NIR-ISL (OM)	0.1767
	The first in NIR-ISL (FeatNet)	0.1721
	Ours (OM)	**0.1611**
	Ours (FeatNet)	**0.1593**

Note: Bold font indicates the best performance in a column.

Fig. 13 Download (/proceedings/DownloadFigures?url=/ContentImages/Journals/JEIME5/31/4/041211/FigureImages/JEI_31_4_041211_f013.png)

DET curves of iris recognition experiments on the CASIA-Iris-Off-angle iris database using different iris segmentation and localization methods.

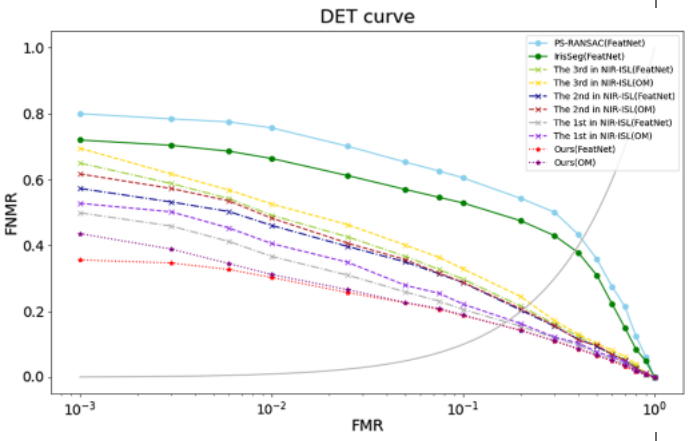

4.4.4. Model applicability

To reflect the model applicability, we report the average running speed and model complexity. Specifically, the proposed IrisGazeSeg reaches a processing speed of 4 FPS for the input of 640×480 pixels. Furthermore, it contains the 336-MB model parameters in total. Overall, the proposed IrisGazeSeg does not show the clear advantageous in term of the real-time and lightweight model. Therefore, we would improve the model applicability in future research.

4.4.5. Ablation study

We also perform the ablation study to verify some important designs of our proposed IrisGazeSeg. The segmentation performance under several ablation settings are mainly analyzed, as tabulated in Table 6 (/journals/journal-of-electronic-imaging/volume-31/issue-04/041211/Multitask-deep-active-contour-based-iris-segmentation-for-off-angle/10.1117/1.JEI.31.4.041211.full#t006). Here IrisGazeSeg (BBox constraints) denotes that IrisGazeSeg jointly predicts the BBox and segmentation mask of iris, and the BBox is used to constrain the valid iris region in the postprocessing. On the basis of IrisGazeSeg (BBox constraints), the IrisGazeSeg (BBox constraints + contours constraints) denotes that IrisGazeSeg further predicts the inner and outer boundaries (contours) of the iris and uses them to constrain the valid iris region in the postprocessing. Furthermore, IrisGazeSeg (BBox constraints + contours constraints + ECA + SoftPool) improves the segmentation branch originally from the DeeplabV3+[35] (/journals/journal-of-electronic-imaging/volume-31/issue-04/041211/Multitask-deep-active-contour-based-iris-segmentation-for-off-angle/10.1117/1.JEI.31.4.041211.full#r35) by employing recent ECA and SoftPool modules, which is also the final IrisGazeSeg model.

Table 6

Experimental results of iris segmentation under several ablation settings.

Dataset	Method	E1 (%)	E2 (%)	F1 (%)
SBVPI	IrisGazeSeg (BBox constraints)	1.02	0.58	89.73
	IrisGazeSeg (BBox constraints + contours constraints)	0.97	0.51	90.07
	IrisGazeSeg (BBox constraints + contours constraints + ECA)	0.92	0.43	90.73
	IrisGazeSeg (BBox constraints + contours constraints + ECA + SoftPool)	**0.89**	**0.37**	**91.43**

CASIA-Iris-Off-angle	IrisGazeSeg (BBox constraints)	0.98	0.52	89.94
	IrisGazeSeg (BBox constraints + contours constraints)	0.94	0.47	90.35
	IrisGazeSeg (BBox constraints + contours constraints + ECA)	0.86	0.43	91.97
	IrisGazeSeg (BBox constraints + contours constraints + ECA + SoftPool)	**0.67**	**0.35**	**93.37**
CASIA-Iris-Africa	IrisGazeSeg (BBox constraints)	1.65	0.87	89.31
	IrisGazeSeg (BBox constraints + contours constraints)	1.57	0.79	89.39
	IrisGazeSeg (BBox constraints + contours constraints + ECA)	0.93	0.55	89.96
	IrisGazeSeg (BBox constraints + contours constraints + ECA + SoftPool)	**0.71**	**0.51**	**92.36**

Note: Bold font indicates the best performance in a column.

It can be seen that by constantly adding new modules, the segmentation performance of IrisGazeSeg achieves an incremental improvement, showing the effectiveness of our introduced BBox detection, deep active contour-based boundary localization, and ECA and SoftPool in the segmentation branch.

4.4.6. Hard cases

In the experiments, we find that there are still some iris images that are not well localized or segmented. Figure 14 (/journals/journal-of-electronic-imaging/volume-31/issue-04/041211/Multitask-deep-active-contour-based-iris-segmentation-for-off-angle/10.1117/1.JEI.31.4.041211.full#f14) shows several poor prediction results. It can be seen that when the degree of off-angle is too large or the eyelid covers most of the iris region, the iris segmentation, especially iris localization has become harder, resulting in a poor prediction.

Fig. 14 Download (/proceedings/DownloadFigures?url=/ContentImages/Journals/JEIME5/31/4/041211/FigureImages/JEI_31_4_041211_f014.png)

Poor prediction results of our method tested on different datasets.

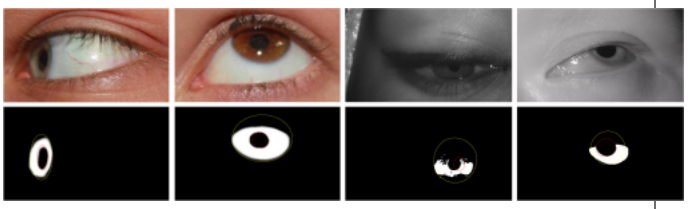

5. Conclusions and Future Work

In this paper, we propose a multitask deep active contour model IrisGazeSeg for segmenting off-angle iris images. Specially, it combines the advantages of deep learning and traditional active contour method and accurately localizes irregular inner and outer boundary contours of the iris for off-angle iris images. Besides, it also improves the DeeplabV3+-based segmentation branch using the recent ECA and SoftPool modules. Finally, an effective postprocessing procedure incorporating the coarse and fine iris localization results to constrain the segmentation result is proposed. Experimental results on both VIS and NIR datasets demonstrate the effectiveness and superiority of our proposed IrisGazeSeg model. In future work, we will explore effective strategies to reduce the model size and improve the running speed. In addition, some new models such as transformer would be also considered to replace/combine CNN-based frameworks to achieve better iris recognition performance.

Acknowledgments

This work was supported by the National Natural Science Foundation of China (Grant Nos. 62106015, U1836217, 62006225, 62071468, and 61906199) and the Beijing University of Civil Engineering and Architecture Research Capacity Promotion Program for Young Scholars (Grant No. X21079). We would like to thank Yong He (Institute of Automation, Chinese Academy of Sciences) and Sida Peng (Zhejiang University) for their support of this work!

References

1. J. Daugman, “High confidence visual recognition of persons by a test of statistical independence,” IEEE Trans. Pattern Anal. Mach. Intell., 15 1148 –1161 (1993). https://doi.org/10.1109/34.244676 (https://doi.org/10.1109/34.244676) ITPIDJ 0162-8828 Google Scholar (http://scholar.google.com/scholar_lookup?title=High+confidence+visual+recognition+of+persons+by+a+test+of+statistical+independence&author=J.+Daugman&journal=IEEE+Trans.+Pattern+Anal.+Mach.+Intell.&volume=15&publication_year=1993&pages=1148-1161)

2. R. Wildes, “Iris recognition: an emerging biometric technology,” Proc. IEEE, 85 1348 –1363 (1997). https://doi.org/10.1109/5.628669 (https://doi.org/10.1109/5.628669) IEEPAD 0018-9219 Google Scholar (http://scholar.google.com/scholar_lookup?title=Iris+recognition:+an+emerging+biometric+technology&author=R.+Wildes&journal=Proc.+IEEE&volume=85&publication_year=1997&pages=1348-1363)

3. Z. Zhao and K. Ajay, “An accurate iris segmentation framework under relaxed imaging constraints using total variation model,” in Proc. IEEE Int. Conf. Comput. Vision, 3828 –3836 (2015). https://doi.org/10.1109/ICCV.2015.436 (https://doi.org/10.1109/ICCV.2015.436) Google Scholar (http://scholar.google.com/scholar_lookup?title=An+accurate+iris+segmentation+framework+under+relaxed+imaging+constraints+using+total+variation+model&author=Z.+Zhao&author=K.+Ajay&conference=Proc.+IEEE+Int.+Conf.+Comput.+Vision&publication_year=2015&pages=3828-3836)

4. T. Tan, Z. He and Z. Sun, “Efficient and robust segmentation of noisy iris images for non-cooperative iris recognition,” Image Vis. Comput., 28 223 –230 (2010). https://doi.org/10.1016/j.imavis.2009.05.008 (https://doi.org/10.1016/j.imavis.2009.05.008) Google Scholar (http://scholar.google.com/scholar_lookup?title=Efficient+and+robust+segmentation+of+noisy+iris+images+for+non-cooperative+iris+recognition&author=T.+Tan&author=Z.+He&author=Z.+Sun&journal=Image+Vis.+Comput.&volume=28&publication_year=2010&pages=223-230)

5. H. Proença and L. A. Alexandre, “Iris segmentation methodology for non-cooperative recognition,” IEE Proc., 153 (2), 199 –205 (2006). https://doi.org/10.1049/ip-vis:20050213 (https://doi.org/10.1049/ip-vis:20050213) Google Scholar (http://scholar.google.com/scholar_lookup?title=Iris+segmentation+methodology+for+non-cooperative+recognition&author=H.+Proença&author=L.+A.+Alexandre&journal=IEE+Proc.&volume=153&issue=2&publication_year=2006&pages=199-205)

6. G. Sutra, S. Garcia-Salicetti and B. Dorizzi, “The Viterbi algorithm at different resolutions for enhanced iris segmentation,” in 5th IAPR Int. Conf. Biom., 310 –316 (2012). https://doi.org/10.1109/ICB.2012.6199825 (https://doi.org/10.1109/ICB.2012.6199825) Google Scholar (http://scholar.google.com/scholar_lookup?title=The+Viterbi+algorithm+at+different+resolutions+for+enhanced+iris+segmentation&author=G.+Sutra&author=S.+Garcia-Salicetti&author=B.+Dorizzi&conference=5th+IAPR+Int.+Conf.+Biom.&publication_year=2012&pages=310-316)

7. S. Banerjee and D. Mery, “Iris segmentation using geodesic active contours and grabcut,” Lect. Notes Comput. Sci., 9555 48 –60 (2016). https://doi.org/10.1007/978-3-319-30285-0_5 (https://doi.org/10.1007/978-3-319-30285-0_5) LNCSD9 0302-9743 Google Scholar (http://scholar.google.com/scholar_lookup?title=Iris+segmentation+using+geodesic+active+contours+and+grabcut&author=S.+Banerjee&author=D.+Mery&journal=Lect.+Notes+Comput.+Sci.&volume=9555&publication_year=2016&pages=48-60)

8. R. D. Labati et al., “Non-ideal iris segmentation using polar spline Ransac and illumination compensation,” Comput. Vision Image Understanding, 188 102787 (2019). https://doi.org/10.1016/j.cviu.2019.07.007 (https://doi.org/10.1016/j.cviu.2019.07.007) CVIUF4 1077-3142 Google Scholar (http://scholar.google.com/scholar_lookup?title=Non-ideal+iris+segmentation+using+polar+spline+Ransac+and+illumination+compensation&author=R.+D.+Labati&journal=Comput.+Vision+Image+Understanding&volume=188&publication_year=2019&pages=102787)

9. S. Shah and A. Ross, “Iris segmentation using geodesic active contours,” IEEE Trans. Inf. Forensics Secur., 4 (4), 824 –836 (2009). https://doi.org/10.1109/TIFS.2009.2033225 (https://doi.org/10.1109/TIFS.2009.2033225) Google Scholar (http://scholar.google.com/scholar_lookup?title=Iris+segmentation+using+geodesic+active+contours&author=S.+Shah&author=A.+Ross&journal=IEEE+Trans.+Inf.+Forensics+Secur.&volume=4&issue=4&publication_year=2009&pages=824-836)

10. C.-W. Tan and A. Kumar, “Unified framework for automated iris segmentation using distantly acquired face images,” IEEE Trans. Image Process., 21 4068 –4079 (2012). https://doi.org/10.1109/TIP.2012.2199125 (https://doi.org/10.1109/TIP.2012.2199125) IIPRE4 1057-7149 Google Scholar (http://scholar.google.com/scholar_lookup?title=Unified+framework+for+automated+iris+segmentation+using+distantly+acquired+face+images&author=C.-W.+Tan&author=A.+Kumar&journal=IEEE+Trans.+Image+Process.&volume=21&publication_year=2012&pages=4068-4079)

11. A. Radman, N. Zainal and S. A. Suandi, “Automated segmentation of iris images acquired in an unconstrained environment using Hog-SVM and growcut,” Digit. Signal Process., 64 60 –70 (2017). https://doi.org/10.1016/j.dsp.2017.02.003 (https://doi.org/10.1016/j.dsp.2017.02.003) DSPREJ 1051-2004 Google Scholar (http://scholar.google.com/scholar_lookup?title=Automated+segmentation+of+iris+images+acquired+in+an+unconstrained+environment+using+Hog-SVM+and+growcut&author=A.+Radman&author=N.+Zainal&author=S.+A.+Suandi&journal=Digit.+Signal+Process.&volume=64&publication_year=2017&pages=60-70)

12. N. Liu et al., “Accurate iris segmentation in non-cooperative environments using fully convolutional networks,” in Int. Conf. Biom., 1 –8 (2016). https://doi.org/10.1109/ICB.2016.7550055 (https://doi.org/10.1109/ICB.2016.7550055) Google Scholar (http://scholar.google.com/scholar_lookup?title=Accurate+iris+segmentation+in+non-cooperative+environments+using+fully+convolutional+networks&author=N.+Liu&conference=Int.+Conf.+Biom.&publication_year=2016&pages=1-8)

13. S. Lian et al., “Attention guided U-Net for accurate iris segmentation,” J. Vis. Commun. Image Represent., 56 296 –304 (2018). https://doi.org/10.1016/j.jvcir.2018.10.001 (https://doi.org/10.1016/j.jvcir.2018.10.001) JVCRE7 1047-3203 Google Scholar (http://scholar.google.com/scholar_lookup?title=Attention+guided+U-Net+for+accurate+iris+segmentation&author=S.+Lian&journal=J.+Vis.+Commun.+Image+Represent.&volume=56&publication_year=2018&pages=296-304)

14. Y.-H. Li et al., “Robust iris segmentation algorithm in non-cooperative environments using interleaved residual U-Net,” Sensors, 21 (4), 1434 (2021). https://doi.org/10.3390/s21041434 (https://doi.org/10.3390/s21041434) SNSRES 0746-9462 Google Scholar (http://scholar.google.com/scholar_lookup?title=Robust+iris+segmentation+algorithm+in+non-cooperative+environments+using+interleaved+residual+U-Net&author=Y.-H.+Li&journal=Sensors&volume=21&issue=4&publication_year=2021&pages=1434)

15. C. Wang et al., “Towards complete and accurate iris segmentation using deep multi-task attention network for non-cooperative iris recognition,” IEEE Trans. Inf. Forensics Secur., 15 2944 –2959 (2020). https://doi.org/10.1109/TIFS.2020.2980791 (https://doi.org/10.1109/TIFS.2020.2980791) Google Scholar (http://scholar.google.com/scholar_lookup?title=Towards+complete+and+accurate+iris+segmentation+using+deep+multi-task+attention+network+for+non-cooperative+iris+recognition&author=C.+Wang&journal=IEEE+Trans.+Inf.+Forensics+Secur.&volume=15&publication_year=2020&pages=2944-2959)

16. X. Feng et al., “Iris R-CNN: accurate iris segmentation and localization in non-cooperative environment with visible illumination,” Pattern Recognit. Lett., (2021). https://doi.org/10.1016/j.patrec.2021.10.031 (https://doi.org/10.1016/j.patrec.2021.10.031) PRLEDG 0167-8655 Google Scholar (http://scholar.google.com/scholar_lookup?title=Iris+R-CNN:+accurate+iris+segmentation+and+localization+in+non-cooperative+environment+with+visible+illumination&author=X.+Feng&journal=Pattern+Recognit.+Lett.&publication_year=2021)

17. K. He et al., “Mask R-CNN,” in Proc. IEEE Int. Conf. Computer Vision, 2961 –2969 (2017). https://doi.org/10.1109/ICCV.2017.322 (https://doi.org/10.1109/ICCV.2017.322) Google Scholar (http://scholar.google.com/scholar_lookup?title=Mask+R-CNN&author=K.+He&conference=Proc.+IEEE+Int.+Conf.+Computer+Vision&publication_year=2017&pages=2961-2969)

18. S. Pundlik, D. Woodard and S. Birchfield, “Iris segmentation in non-ideal images using graph cuts,” Image Vis. Comput., 28 (12), 1671 –1681 (2010). https://doi.org/10.1016/j.imavis.2010.05.004 (https://doi.org/10.1016/j.imavis.2010.05.004) Google Scholar (http://scholar.google.com/scholar_lookup?title=Iris+segmentation+in+non-ideal+images+using+graph+cuts&author=S.+Pundlik&author=D.+Woodard&author=S.+Birchfield&journal=Image+Vis.+Comput.&volume=28&issue=12&publication_year=2010&pages=1671-1681)

19. A. Gangwar et al., “IrisSeg: a fast and robust iris segmentation framework for non-ideal iris images,” in Int. Conf. Biom., 1 –8 (2016). https://doi.org/10.1109/ICB.2016.7550096 (https://doi.org/10.1109/ICB.2016.7550096) Google Scholar (http://scholar.google.com/scholar_lookup?title=IrisSeg:+a+fast+and+robust+iris+segmentation+framework+for+non-ideal+iris+images&author=A.+Gangwar&conference=Int.+Conf.+Biom.&publication_year=2016&pages=1-8)

20. M. A. Abdullah et al., “Robust iris segmentation method based on a new active contour force with a noncircular normalization,” IEEE Trans. Syst. Man Cybern. Syst., 47 (12), 3128 –3141 (2017). https://doi.org/10.1109/TSMC.2016.2562500 (https://doi.org/10.1109/TSMC.2016.2562500) Google Scholar (http://scholar.google.com/scholar_lookup?title=Robust+iris+segmentation+method+based+on+a+new+active+contour+force+with+a+noncircular+normalization&author=M.+A.+Abdullah&journal=IEEE+Trans.+Syst.+Man+Cybern.+Syst.&volume=47&issue=12&publication_year=2017&pages=3128-3141)

21. H. Fathee and S. Sahmoud, “Iris segmentation in uncooperative and unconstrained environments: state-of-the-art, datasets and future research directions,” Digit. Signal Process., 118 103244 (2021). https://doi.org/10.1016/j.dsp.2021.103244 (https://doi.org/10.1016/j.dsp.2021.103244) DSPREJ 1051-2004 Google Scholar (http://scholar.google.com/scholar_lookup?title=Iris+segmentation+in+uncooperative+and+unconstrained+environments:+state-of-the-art,+datasets+and+future+research+directions&author=H.+Fathee&author=S.+Sahmoud&journal=Digit.+Signal+Process.&volume=118&publication_year=2021&pages=103244)

22. M. Arsalan et al., “FRED-Net: fully residual encoder–decoder network for accurate iris segmentation,” Expert Syst. Appl., 122 217 –241 (2019). https://doi.org/10.1016/j.eswa.2019.01.010 (https://doi.org/10.1016/j.eswa.2019.01.010) Google Scholar (http://scholar.google.com/scholar_lookup?title=FRED-Net:+fully+residual+encoder–decoder+network+for+accurate+iris+segmentation&author=M.+Arsalan&journal=Expert+Syst.+Appl.&volume=122&publication_year=2019&pages=217-241)

23. R. R. Jha et al., “PixISegNet: pixel-level iris segmentation network using convolutional encoder–decoder with stacked hourglass bottleneck,” IET Biom., 9 (1), 11 –24 (2020). https://doi.org/10.1049/iet-bmt.2019.0025 (https://doi.org/10.1049/iet-bmt.2019.0025) Google Scholar (http://scholar.google.com/scholar_lookup?title=PixISegNet:+pixel-level+iris+segmentation+network+using+convolutional+encoder–decoder+with+stacked+hourglass+bottleneck&author=R.+R.+Jha&journal=IET+Biom.&volume=9&issue=1&publication_year=2020&pages=11-24)

24. V. Varkarakis, S. Bazrafkan and P. Corcoran, “Deep neural network and data augmentation methodology for off-axis iris segmentation in wearable headsets,” Neural Netw., 121 101 –121 (2020). https://doi.org/10.1016/j.neunet.2019.07.020 (https://doi.org/10.1016/j.neunet.2019.07.020) NNETEB 0893-6080 Google Scholar (http://scholar.google.com/scholar_lookup?title=Deep+neural+network+and+data+augmentation+methodology+for+off-axis+iris+segmentation+in+wearable+headsets&author=V.+Varkarakis&author=S.+Bazrafkan&author=P.+Corcoran&journal=Neural+Netw.&volume=121&publication_year=2020&pages=101-121)

25. H. Hofbauer, E. Jalilian and A. Uhl, “Exploiting superior CNN-based iris segmentation for better recognition accuracy,” Pattern Recognit. Lett., 120 17 –23 (2019). https://doi.org/10.1016/j.patrec.2018.12.021 (https://doi.org/10.1016/j.patrec.2018.12.021) PRLEDG 0167-8655 Google Scholar (http://scholar.google.com/scholar_lookup?title=Exploiting+superior+CNN-based+iris+segmentation+for+better+recognition+accuracy&author=H.+Hofbauer&author=E.+Jalilian&author=A.+Uhl&journal=Pattern+Recognit.+Lett.&volume=120&publication_year=2019&pages=17-23)

26. E. Jalilian, M. Karakaya and A. Uhl, “End-to-end off-angle iris recognition using CNN based iris segmentation,” in Int. Conf. Biom. Special Interest Group, 1 –7 (2020). Google Scholar (http://scholar.google.com/scholar_lookup?title=End-to-end+off-angle+iris+recognition+using+CNN+based+iris+segmentation&author=E.+Jalilian&author=M.+Karakaya&author=A.+Uhl&conference=Int.+Conf.+Biom.+Special+Interest+Group&publication_year=2020&pages=1-7)

27. J. E. Tapia et al., “Semantic segmentation of periocular near-infra-red eye images under alcohol effects,” IEEE Access, 9 109732 –109744 (2021). https://doi.org/10.1109/ACCESS.2021.3101256 (https://doi.org/10.1109/ACCESS.2021.3101256) Google Scholar (http://scholar.google.com/scholar_lookup?title=Semantic+segmentation+of+periocular+near-infra-red+eye+images+under+alcohol+effects&author=J.+E.+Tapia&journal=IEEE+Access&volume=9&publication_year=2021&pages=109732-109744)

28. C. Wang et al., “NIR iris challenge evaluation in non-cooperative environments: segmentation and localization,” in IEEE Int. Joint Conf. Biom., 1 –10 (2021). https://doi.org/10.1109/IJCB52358.2021.9484336 (https://doi.org/10.1109/IJCB52358.2021.9484336) Google Scholar (http://scholar.google.com/scholar_lookup?title=NIR+iris+challenge+evaluation+in+non-cooperative+environments:+segmentation+and+localization&author=C.+Wang&conference=IEEE+Int.+Joint+Conf.+Biom.&publication_year=2021&pages=1-10)

29. Z. Sun and T. Tan, “Ordinal measures for iris recognition,” IEEE Trans. Pattern Anal. Mach. Intell., 31 (12), 2211 –2226 (2008). https://doi.org/10.1109/TPAMI.2008.240 (https://doi.org/10.1109/TPAMI.2008.240) ITPIDJ 0162-8828 Google Scholar (http://scholar.google.com/scholar_lookup?title=Ordinal+measures+for+iris+recognition&author=Z.+Sun&author=T.+Tan&journal=IEEE+Trans.+Pattern+Anal.+Mach.+Intell.&volume=31&issue=12&publication_year=2008&pages=2211-2226)

30. Z. Zhao and A. Kumar, “Towards more accurate iris recognition using deeply learned spatially corresponding features,” in Proc. IEEE Int. Conf. Comput. Vision, 3809 –3818 (2017). https://doi.org/10.1109/ICCV.2017.411 (https://doi.org/10.1109/ICCV.2017.411) Google Scholar (http://scholar.google.com/scholar_lookup?title=Towards+more+accurate+iris+recognition+using+deeply+learned+spatially+corresponding+features&author=Z.+Zhao&author=A.+Kumar&conference=Proc.+IEEE+Int.+Conf.+Comput.+Vision&publication_year=2017&pages=3809-3818)

31. M. Sandler et al., “MobileNetV2: inverted residuals and linear bottlenecks,” in Proc. IEEE Conf. Comput. Vision and Pattern Recognit., 4510 –4520 (2018). https://doi.org/10.1109/CVPR.2018.00474 (https://doi.org/10.1109/CVPR.2018.00474) Google Scholar (http://scholar.google.com/scholar_lookup?title=MobileNetV2:+inverted+residuals+and+linear+bottlenecks&author=M.+Sandler&conference=Proc.+IEEE+Conf.+Comput.+Vision+and+Pattern+Recognit.&publication_year=2018&pages=4510-4520)

32. S. Peng et al., “Deep snake for real-time instance segmentation,” in Proc. IEEE/CVF Conf. Comput. Vision and Pattern Recognit., 8533 –8542 (2020). https://doi.org/10.1109/CVPR42600.2020.00856 (https://doi.org/10.1109/CVPR42600.2020.00856) Google Scholar (http://scholar.google.com/scholar_lookup?title=Deep+snake+for+real-time+instance+segmentation&author=S.+Peng&conference=Proc.+IEEE/CVF+Conf.+Comput.+Vision+and+Pattern+Recognit.&publication_year=2020&pages=8533-8542)

33. X. Zhou, D. Wang and P. Krähenbühl, “Objects as points,” (2019). Google Scholar (http://scholar.google.com/scholar_lookup?title=Objects+as+points&author=X.+Zhou&author=D.+Wang&author=P.+Krähenbühl&publication_year=2019)

34. L.-C. Chen et al., “Encoder-decoder with atrous separable convolution for semantic image segmentation,” Lect. Notes Comput. Sci., 11211 801 –818 (2018). https://doi.org/10.1007/978-3-030-01234-2_49 (https://doi.org/10.1007/978-3-030-01234-2_49) LNCSD9 0302-9743 Google Scholar (http://scholar.google.com/scholar_lookup?title=Encoder-decoder+with+atrous+separable+convolution+for+semantic+image+segmentation&author=L.-C.+Chen&journal=Lect.+Notes+Comput.+Sci.&volume=11211&publication_year=2018&pages=801-818)

35. A. Stergiou, R. Poppe and G. Kalliatakis, “Refining activation downsampling with softpool,” in Proc. IEEE Int. Conf. Comput. Vision, (2021). Google Scholar (http://scholar.google.com/scholar_lookup?title=Refining+activation+downsampling+with+softpool&author=A.+Stergiou&author=R.+Poppe&author=G.+Kalliatakis&conference=Proc.+IEEE+Int.+Conf.+Comput.+Vision&publication_year=2021)

36. Q. Wang et al., “ECA-Net: efficient channel attention for deep convolutional neural networks,” in Proc. IEEE Conf. Comput. Vision and Pattern Recognit., (2020). https://doi.org/10.1109/CVPR42600.2020.01155 (https://doi.org/10.1109/CVPR42600.2020.01155) Google Scholar (http://scholar.google.com/scholar_lookup?title=ECA-Net:+efficient+channel+attention+for+deep+convolutional+neural+networks&author=Q.+Wang&conference=Proc.+IEEE+Conf.+Comput.+Vision+and+Pattern+Recognit.&publication_year=2020)

37. J. Hu, L. Shen and G. Sun, “Squeeze-and-excitation networks,” in Proc. IEEE Conf. Comput. Vision and Pattern Recognit., 7132 –7141 (2018). https://doi.org/10.1109/CVPR.2018.00745 (https://doi.org/10.1109/CVPR.2018.00745) Google Scholar (http://scholar.google.com/scholar_lookup?title=Squeeze-and-excitation+networks&author=J.+Hu&author=L.+Shen&author=G.+Sun&conference=Proc.+IEEE+Conf.+Comput.+Vision+and+Pattern+Recognit.&publication_year=2018&pages=7132-7141)

38. R. Girshick, “Fast R-CNN,” in Proc. IEEE Int. Conf. Comput. Vision, 1440 –1448 (2015). https://doi.org/10.1109/ICCV.2015.169 (https://doi.org/10.1109/ICCV.2015.169) Google Scholar (http://scholar.google.com/scholar_lookup?title=Fast+R-CNN&author=R.+Girshick&conference=Proc.+IEEE+Int.+Conf.+Comput.+Vision&publication_year=2015&pages=1440-1448)

39. T.-Y. Lin et al., “Focal loss for dense object detection,” in Proc. IEEE Int. Conf. Comput. Vision, 2980 –2988 (2017). https://doi.org/10.1109/ICCV.2017.324 (https://doi.org/10.1109/ICCV.2017.324) Google Scholar (http://scholar.google.com/scholar_lookup?title=Focal+loss+for+dense+object+detection&author=T.-Y.+Lin&conference=Proc.+IEEE+Int.+Conf.+Comput.+Vision&publication_year=2017&pages=2980-2988)

40. M. Vitek et al., “A comprehensive investigation into sclera biometrics: a novel dataset and performance study,” Neural Comput. Appl., 32 17941 –17955 (2020). https://doi.org/10.1007/s00521-020-04782-1 (https://doi.org/10.1007/s00521-020-04782-1) Google Scholar (http://scholar.google.com/scholar_lookup?title=A+comprehensive+investigation+into+sclera+biometrics:+a+novel+dataset+and+performance+study&author=M.+Vitek&journal=Neural+Comput.+Appl.&volume=32&publication_year=2020&pages=17941-17955)

41. J. Hu et al., “A large-scale database for less cooperative iris recognition,” in IEEE Int. Joint Conf. Biom., 1 –6 (2021). https://doi.org/10.1109/IJCB52358.2021.9484357 (https://doi.org/10.1109/IJCB52358.2021.9484357) Google Scholar (http://scholar.google.com/scholar_lookup?title=A+large-scale+database+for+less+cooperative+iris+recognition&author=J.+Hu&conference=IEEE+Int.+Joint+Conf.+Biom.&publication_year=2021&pages=1-6)

42. H. Proença and L. A. Alexandre, “The NICE. I: noisy iris challenge evaluation-part I,” in Proc. IEEE Int. Conf. Biom.: Theory, Appl., and Syst., 1 –4 (2007). https://doi.org/10.1109/BTAS.2007.4401910 (https://doi.org/10.1109/BTAS.2007.4401910) Google Scholar (http://scholar.google.com/scholar_lookup?title=The+NICE.+I:+noisy+iris+challenge+evaluation-part+I&author=H.+Proença&author=L.+A.+Alexandre&conference=Proc.+IEEE+Int.+Conf.+Biom.:+Theory,+Appl.,+and+Syst.&publication_year=2007&pages=1-4)

Biography

Tianhao Lu received his BE degree in communication engineering from Beijing Jiaotong University, China, in 2017. He is currently pursuing his MS degree with Hunan University of Technology, and also an intern at the Center for Research on Intelligent Perception and Computing, National Laboratory of Pattern Recognition, Institute of Automation, Chinese Academy of Sciences. His research interests include biometrics and computer vision.

Caiyong Wang received his BE degree in applied mathematics from Xinjiang University, China, in 2013, his MS degree in computational mathematics from Xiamen University, China, in 2016, and his PhD in pattern recognition and intelligent systems from the Institute of Automation, Chinese Academy of Sciences in 2020. He is currently a lecturer with the School of Electrical and Information Engineering, Beijing University of Civil Engineering and Architecture, China, and also with the Beijing Key Laboratory of Intelligent Processing for Building Big Data, China. His current research interests include biometrics, computer vision, and deep learning. He has received an Honorable Mention Paper Award at IAPR ICB 2019.

Yunlong Wang received his BE and PhD degrees from the Department of Automation, University of Science and Technology of China. He is currently an assistant professor with the Center for Research on Intelligent Perception and Computing, National Laboratory of Pattern Recognition, Institute of Automation, Chinese Academy of Sciences. His research focuses on pattern recognition, machine learning, light field photography, and biometrics.

Zhenan Sun received his BE degree in industrial automation from Dalian University of Technology, China, in 1999, his MS degree in system engineering from the Huazhong University of Science and Technology, China, in 2002, and his PhD in pattern recognition and intelligent systems from the Institute of Automation, Chinese Academy of Sciences, China, in 2006. He is currently a professor with the Center for Research on Intelligent Perception and Computing, National Laboratory of Pattern Recognition, Institute of Automation, Chinese Academy of Sciences, and also with the School of Artificial Intelligence, University of Chinese Academy of Sciences, China. He has authored/coauthored over 200 technical papers. His research interests include biometrics, pattern recognition, and computer vision. He is the chair of technical committee on biometrics, Int. Association for Pattern Recognition (IAPR), and an IAPR fellow. He serves as an associate editor for the IEEE Transactions on Biometrics, Behavior, and Identity Science (IEEE TBIOM).

Citation

Received: 5 October 2021; Accepted: 11 February 2022; Published: 26 February 2022